LONG TERM SOIL MOISTURE MONITORING AND ASSESSING THEORETICAL DATA INTERPRETATION TECHNIQUES USING HEATED DISTRIBUTED TEMPERATURE SENSING

By

John J. Sourbeer

A Thesis submitted in partial fulfillment of

the requirements for the degree of

Master of Science

(Civil and Environmental Engineering – Water Resources Engineering)

at the

UNIVERSITY OF WISCONSIN – MADISON

2013

Abstract

Soil moisture (θ) is an important component of the hydrologic cycle. This key variable has complex spatial and temporal dynamics, but current measurement techniques cannot feasibly provide θ estimate at both high spatial and temporal resolution at the landscape scale. A better understanding of θ dynamics could lead to a broad range of scientific insights, and θ monitoring at high spatial and temporal resolutions could provide many societal benefits such as improving flood forecasting, precision agriculture, and landfill leakage detection. Heated distributed temperature sensing (DTS) using fiber optics has the potential to fill this gap in θ monitoring at the landscape scale. This technology has the capability of estimating θ at 1 meter spatial resolution and sub-daily temporal resolution over 10 km. For over a decade, attempts have been made to implement heated DTS systems to estimate θ, but there have yet to be any long term studies and a variety of data interpretation techniques have been proposed.

A field deployed heated DTS system was deployed at the East Branch Pecatonica River Hydroecologic Observatory in the summer of 2010. Data obtained from this heated DTS system from September 2010 to September 2013 was used to assess the feasibility of estimating θ with this technology. Effects of thermal hysteresis and soil structure healing were observed in the relationship between the maximum temperature response produced by a heat pulse and independently logging dielectric θ sensors. These two phenomena are related to the pore structure directly surrounding the DTS cable, and both can be described with a contact resistance. A two dimensional finite element model of the DTS cable was used in

addition to the field data to quantify the contact resistance (i.e. air gap) between the cable and soil through time. These estimates identified a θ-dependent and time-dependent contact resistance and showed that the thermal hysteresis and soil structure healing could be quantified by a contact resistance. These findings greatly complicated the relationship between the maximum temperature response and θ and led to the pursuit of alternative data interpretation techniques. The finite element model was then used to simulate various θ and contact resistance conditions. These model results were used to propose two theoretical data interpretation techniques to estimating θ despite the presence of a fluctuating contact resistance.

Acknowledgements

First, I would like to thank Steve Loheide for being a great advisor. He was always available to discuss any questions or concerns I had. When I first arrived in Wisconsin, Steve explained a range of topics that I could pursue at the East Branch Pecatonica (EBP) River Hydroecologic Observatory. He always gave thoughtful advice as I proposed ideas. When I had results or questions, he was always available to discuss them, and after our meetings, I would feel encouraged and driven to keep working diligently. I truly appreciate Steve's help and direction in earning my degree and challenging me in ways that have enabled me to grow professionally.

I would also like to thank Professor Ken Potter and Professor Sam Kung for being on my defense committee. It was great working with them through classes and research during my tenure at UW.

This work would not have been possible without the support of Steve Richter from The Nature Conservancy (TNC). He facilitated our use of TNC property to conduct the field component of this research. I would also like to thank Eric Mark for checking in with me to ensure TNC maintenance work did not damage or conflict with the research being conducted at EBP.

Arlen Striegl developed this DTS system before I arrived, so I would like to acknowledge his work that my thesis is based upon. Arlen also was available to help me with data processing questions that came up via email and even helped me in person when he returned to UW for a

visit during my first semester. Jeff Miller was also very supportive in helping me interpret data processing code in MATLAB.

Matt Weber and Eric Booth were pivotal in introducing me to the field work and data collection at EBP. Matt was key in transitioning the maintenance of the DTS system from Arlen to me. Eric was always available to answer questions I had about more general data collection activities at EBP, and he made himself available to walk me through the data collection process in person during my first semester. On a parallel note, I would like to thank Carolyn Voter for taking the role of data collection and maintenance at EBP during my final semester and into the future. I would also like to acknowledge everyone from the Hydroecology group who provided thoughtful feedback to this research at various points in my tenure at UW. I would also like to thank the larger WRE group for giving me feedback during my seminar presentations and giving me feedback at various moments around the office or during conferences.

My family was always supportive through conversations over the phone and by providing a relaxing atmosphere back home when I was able to visit. The diligent attitude that has enabled me to get through the strenuous moments as a grad student is a characteristic I picked up from them. Hard work was stressed as a necessary trait for success in any activity, and completing a job well rather than simply completing a job has helped me follow through with many tough assignments to complete a product I can be proud of.

Lastly, I would like to thank Amanda for helping me through so many moments over the past two years. Being available to chat about my day certainly eased my stress. Also, giving me

feedback on my writing, presentations, and research decisions certainly improved my work. Traveling all the way from NYC to visit me several times during my time in Wisconsin gave me the opportunity to relax and enjoy my surroundings. Thank you for patiently working through the tough times with me. I look forward to our future together.

Contents

Chapter 1: Introduction

1.1. Problem Statement

Soil moisture (θ) is a critical component of the hydrologic cycle. It is also a key factor influencing land-atmosphere interactions. θ data at high spatial and temporal resolutions could be used for a wide range of applications such as improving the scientific understanding of soil moisture dynamics, improving meteorological and climate forecasting, and improving risk assessments of flooding and drought (Ochsner et al., 2013). Unfortunately, obtaining this data can become time consuming and expensive using conventional technology. Point measurement sensors can obtain high temporal resolutions, but deploying large quantities of these sensors to obtain high spatial resolution can become expensive. Remote satellite and aerial imagery can provide θ estimates over large areas, but with low spatial and temporal resolutions. In the past decade, heated distributed temperature sensing (DTS) using fiber optics has shown potential to fill this gap (Sayde et al., 2010; Striegl and Loheide, 2012), but there have yet to be any long term studies testing the precision and accuracy of this technology. There has also been varying strategies to interpret heated DTS data to provide accurate and precise estimates of θ (Sayde et al., 2010; Striegl and Loheide, 2012; Weiss, 2003).

1.2. Project Concept

A heated DTS system was installed in the summer of 2010 with several independently logging dielectric θ sensors (Striegl and Loheide, 2012; Striegl, 2011). Since installation, this system has provided a large amount of data, which can be analyzed to determine the

effectiveness of using DTS technology to estimate θ. Also, a two dimensional finite element model was developed to help explain the mechanisms behind trends observed in the field data. This model was also used to test alternative data interpretation techniques to potentially overcome obstacles observed in the field data.

1.3. Project Background

1.3.1. Study Site

The study site is located at the East Branch Pecatonica River Hydroecologic Observatory, which is approximately 3 miles south of Barneveld, Wisconsin. The site is in an area of the Midwest known as the Driftless Area. This area did not experience glaciation during the most recent glacial period and is characterized by deeply dissected river valleys. Valley bottoms in this area of Wisconsin typically have three distinct sedimentary layers: basal coarse gravel overlain by silty clay overlain by post-settlement alluvium (Knox, 1972). The post-settlement alluvium was a result of soil erosion caused by intense row cropping and grazing of the native grasslands and oak savannahs during the late 1800s and early 1900s by European settlers. This change in land cover caused major shifts in the hydrology and ecology of the landscape. Post-settlement alluvium was deposited across the floodplains and increased the channel bank height, which effectively disconnected the floodplains from the channels. Moderate floods no longer spilled over the banks into the floodplains, and water is quickly routed downstream. This additional sediment increased the depth to groundwater in the floodplains, which altered the subsurface hydrology. These hydrologic shifts and land use changes caused major shifts in the ecosystem function. The most notable ecological shift in

the Driftless Area floodplains was the transition from wet meadow grasses and forb species to drier, woody species.

In recent decades, restoration efforts have been made to restore these ecosystems to pre-settlement conditions. In 2006, The Nature Conservancy (TNC) and the Wisconsin Department of Natural Resources (WDNR) completed a novel "scrape" restoration technique at the current site of the East Branch Pecatonica Hydroecologic Observatory. The post-settlement alluvium was removed using large earth-movers to restore the pre-settlement topography of the floodplain. The objectives of this restoration project were to restore the connection between the channel and the floodplain and decrease the depth to groundwater (Booth et al., 2009). Native plant seed mix was spread to reestablish native vegetation communities and encourage restoration of the ecosystem function.

Following restoration, efforts were made to collect hydrologic and ecologic data to assess the effects of the restoration. The depth to groundwater was decreased, but surprisingly, the unsaturated (root) zone actually experienced drier conditions than a nearby unrestored floodplain (Booth and Loheide, 2010). In particular, an area west of the stream developed a band of especially dry soil in the central zone of the floodplain. Booth and Loheide (2010) found that the drier central zone was caused by a spatially discontinuous silt-clay confining layer below the root zone that prevents groundwater from upwelling into the root zone. This area provided an opportunity to observe spatial gradients in θ with a heated DTS system. The chosen transect for the DTS cable was found to have a nearly homogeneous silt loam soil down to a depth of 30-50 cm. The strong spatial and temporal variability in θ across this

transect provided an opportunity to test the effectiveness of a heated DTS system to capture these θ dynamics.

1.3.2. Heated DTS System Design

The custom design for the heated DTS cable used at the East Branch Pecatonica River Hydroecologic Observatory conceptually resembles a single probe heat pulse (SPHP) sensor. SPHP sensors consist of a single probe, which has the capability of generating a heat pulse and monitoring the temperature response. This DTS cable consists of fiber optics (capable of monitoring temperature) bundled with resistive heating and enclosed in a protective polypropylene extrusion. This design was fabricated by Gulf Coast Downhold Technologies (Houston, Texas). The fiber optics are monitored by a Halo DTS processor (Sensornet Ltd. Halo DTS 4 km, BMP Enterprises, Houston, Texas) by transmitting a light pulse down the fiber optics and recording the backscattered light. The backscattered light is dependent on the temperature within the fibers. This system is set-up to take double-ended temperature measurements by connecting two separate fibers via a turnaround. A light pulse is sent down one fiber and returns on another. Directly afterwards, another light pulse is sent down the fiber at which the light pulse returned and returns on the initial fiber. The results of these two sequences are then averaged to represent one temperature trace. The resistive heating is controlled by a custom power control box and timing instrumentation (GC 18SA120 and 7DT-2CH, ISE Inc., Cleveland, Ohio), which has been programmed to generate a 10-minute heat pulse every 2 hours. The power is supplied by a variable transformer (Variac 5021CT-2S, ISE, Inc., Cleveland, Ohio), which transforms a 240 VAC input to a 560 VAC output. This output is constant and equal to 3.07 Wm^{-1}.

This heated DTS system was deployed July 15, 2010. The cable was knifed into the ground at a constant 20 cm depth with a vibratory plow (DitchWitch 100SX) to minimize soil disturbance. Following this process, water was poured over the soil scar to encourage soil structure healing. A small structure was constructed to house the DTS equipment. This structure is well insulated and contains an air conditioner/heater to minimize the effects of temperature fluctuations.

1.4. Objectives and Purpose

The purpose of this thesis is to determine the feasibility of heated DTS to estimate θ by analyzing both field data obtained from September 2010 to September 2013 and model simulations of a heat pulse.

This project is divided into the following two objectives:

I. Determine the feasibility of estimating θ using heated DTS by analyzing over three years of data from a field deployed heated DTS system at the East Branch Pecatonica River Hydroecologic Observatory (south of Barneveld, Wisconsin).

II. Propose theoretical data interpretation techniques to potentially overcome the obstacles observed from the field deployed DTS system using results from a two-dimensional finite element model.

In Chapter 2, which has been submitted to *Hydrological Processes* for review, field data obtained from the heated DTS system is compared to model simulations at varying θ conditions and contact resistances between the cable and soil. Several obstacles to estimating

θ using a metric of the maximum temperature response are identified. All of these obstacles are found to be related to the degree to which the soil is in close contact to the cable. Model simulations are used to quantify this phenomenon through time at one location along the cable. With these obstacles, it is proposed that different data interpretation techniques should be pursued. Chapter 3 uses additional model simulations to identify two general data interpretation techniques that theoretically could be used to estimate θ despite varying degrees of contact between the soil and cable. These results should help inform the data interpretation process for currently deployed heated DTS systems and improve future heated DTS designs. Once these identified problems are addressed, heated DTS systems may better deliver θ estimates at high spatial and temporal resolutions with accuracy and precision.

Chapter 2: Long-term soil moisture monitoring with heated distributed temperature sensing

East Branch Pecatonica River Hydroecologic Observatory

Barneveld, Wisconsin

Note: A manuscript based on this chapter has been submitted to the journal of Hydrological Processes

Abstract

The field deployment of a heated distributed temperature sensor (DTS) for over three years has revealed two obstacles to estimating soil moisture (θ) that may hamper subsurface DTS applications as well as use of other subsurface thermal probes. The first observed obstacle was thermal hysteresis. Thermal hysteresis causes the relationship between θ and the temperature response (ΔT) within the cable to be dependent not only on θ of the soil, but also on the previous wetting and drying cycles leading to that state. The second observed obstacle was soil structure healing. Soil structure healing causes the relationship between ΔT and θ to evolve through time; this calibration curve becomes flatter, or less sensitive, as the surrounding soil makes better contact with the cable. Effects of thermal hysteresis and soil structure healing are largely the result of small gaps between the cable and soil. These small gaps can be approximated by a contact resistance between the cable and soil. The objective of this article is to characterize the occurrence of hysteretic and soil structure healing effects from field data and parameterize contact resistance by simulating heat transfer using a numerical modeling approach.

2.1. Introduction

Distributed temperature sensing (DTS) using fiber optic technology first emerged in the 1980s (Dakin et al., 1985). In the past decade, DTS systems have been used for a variety of hydrologic monitoring applications (Selker et al., 2006; Suárez et al., 2011). There have been several attempts to use this technology to obtain estimates of soil moisture (θ) (Ciocca et al., 2012; Krzeminska et al., 2012; Sayde et al., 2010; Steele-Dunne et al., 2010; Striegl and Loheide, 2012). The primary motivation of this previous work has been to obtain high spatial and high temporal resolution θ data, which would be useful for many hydrologic applications (Ochsner et al., 2013). For example, this type of data could be used to improve rainfall-runoff response predictions (Dunne and Black, 1970), flood forecasting (Casper et al., 2007), turf irrigation (Cardenas-Lailhacar et al., 2008), precision agriculture (Stafford, 2000; Zhang et al., 2002), landfill leakage detection (Khire et al., 1997), knowledge of various ecosystem processes (Knapp et al., 2002)), and hydroecological investigations (Robinson et al., 2008).

High spatial and temporal resolution θ data cannot be easily obtained due to limitations in current measurement capabilities (Robinson et al., 2008). Point measurements (e.g., time domain reflectometry and gravimetric sampling) can be taken to obtain both high spatial and temporal resolution, but this method becomes expensive and time-consuming at a landscape scale. Remote sensing methods can provide estimates of θ over large spatial areas, but with low spatial resolution (Kerr et al., 2001). DTS technology may be able to fill the gap between spatial and temporal scales as research suggests it could provide estimates of θ of lengths up to 10 km with 1-2 m spatial resolution and sub-daily temporal resolution (Selker et al., 2006).

There are two general classes of methods for using DTS to estimate θ. One class of methods involves passively measuring the near-surface temperature fluctuations caused by diurnal radiative heating with multiple DTS cables (Krzeminska et al., 2012; Steele-Dunne et al., 2010). This approach is advantageous in remote areas where power supply is limited, but temperature variations can be reduced by canopy or cloud cover and it can be difficult to place the cables at consistent depths.

The other class of methods involves actively generating a heat pulse and measuring the temperature response (ΔT) with respect to time using a DTS system. ΔT is dependent on the surrounding θ since heat dissipates away from the cable more efficiently in wet conditions than in dry conditions. This dependency is a result of several factors. First, water has a higher thermal conductivity (λ) and higher heat capacity (C_P) than air. Second, water effectively 'bridges' the soil particles to create heat transport pathways, as soil particles have a higher λ than water. These factors cause the bulk λ and C_P of the soil to increase, which respectively, enables heat to transport away from the cable faster and provides more heat storage potential as more water is present in the surrounding soil. Heat pulses have been commonly used to estimate λ with calibrated single-probe heat pulse (SPHP) sensors (de Vries, 1952; Shiozawa and Campbell, 1990). The same theory can be applied to estimating θ as λ is dependent on θ (Shiozawa and Campbell, 1990).

This heat pulse method coupled with a DTS system was first used to determine whether the surrounding soil was dry, wet, or saturated (Perzlmaier et al., 2006, 2004; Weiss, 2003). In recent years, attempts have been made to improve the accuracy and precision of heated DTS systems. Analytical methods similar to the SPHP method have been used to determine the

thermal properties of the soil through analysis of the heating and cooling phase, which can be used to estimate θ (Ciocca et al., 2012). There also have been attempts to use independently logging θ sensors to develop an empirical relationship between θ and ΔT (Sayde et al., 2010; Striegl and Loheide, 2012). This empirical relationship is dependent on the soil type, cable design, and heat pulse. It assumes homogeneous soil and a temporally constant contact resistance between the cable and soil across the length of the cable.

Contact resistance between the cable and soil is common among heat pulse sensors and can be an obstacle to estimating thermal properties, especially with single probe sensors (Blackwell, 1954; de Vries and Peck, 1958; García et al., 1991; Goto and Matsubayashi, 2008; van Haneghem, 1983; Waite et al., 2007, 2006). This obstacle can be circumvented when estimating λ by analyzing the slope of late time ΔT versus log time (Shiozawa and Campbell, 1990). Late time data is a better approximation of the surrounding soil since the influence of the cable properties and contact resistance is minimized at this time. Longer heat pulses are needed to circumvent the effects of larger contact resistances.

Empirical relationships to estimate θ can be developed using a metric such as the maximum temperature response (ΔT_{max}) without a known contact resistance. Developing this relationship can be challenging as the contact resistance must not change through time as ΔT_{max} is dependent on both θ and the contact resistance (Ham and Benson, 2003; Heitman et al., 2003; Song et al., 1998). Unfortunately, contact resistance may be dependent on θ as the surrounding soil swells and shrinks (Song et al., 1998) and the saturation state of the gap between the sensor and the soil changes. An empirical relationship can still be developed in

those situations, but the relationship between contact resistance and θ must not change through time or space. Spatial heterogeneity along the length of the sensor is not often an issue with small, point probes, but a long DTS cable may be more prone to such heterogeneity.

The objective of this article is to use data from a long-term (> 3 years), field-deployed, heated DTS system outlined in Striegl (2011) to identify the mechanisms responsible for error and uncertainty in DTS estimated θ and the underlying cause of shifting of calibration relationships. We will conclude with a discussion of whether these obstacles can be avoided or overcome to estimate θ.

2.2. Materials and Methods

2.2.1. Site Description

The study site is located at the Upper East Branch Pecatonica River Hydroecologic Observatory, which is located within the Driftless Area of southwestern Wisconsin (Figure 2.1). This area was left unglaciated during the Pleistocene and is characterized by branching stream networks bounded by deeply incised valleys. A silt-clay series overlays a gravel, alluvial layer, which overlays bedrock. This laminated silt-clay series cap is post-settlement alluvium which is ubiquitous throughout valley bottoms in the region and typically has reached thicknesses on the order of 30 to 400 cm over the last 200 years (Knox, 2006, 1972). The post-settlement alluvium on the floodplain caused major hydrologic and ecologic regime shifts (Booth and Loheide, 2012a, 2012b; Loheide and Booth, 2011). These shifts prompted a novel restoration technique to re-establish the pre-settlement hydrologic dynamics and ecologic communities.

In 2006, The Nature Conservancy and Wisconsin Department of Natural Resources led restoration efforts to remove the post-settlement alluvium to decrease the depth to the water table and reintroduce wetland habitat (Booth et al., 2009). Once restoration was complete, a distinctive wet-dry-wet pattern developed west of the stream (Figure 2.1a). This dry section is caused by a silt clay layer that behaves like a confining unit (Hunt et al., 1999), which effectively prevents groundwater in the gravel layer from upwelling to the near-surface soil zone. This wet-dry-wet pattern provided an opportunity to observe spatial variations in θ with heated DTS technology. A heated DTS system was installed in the summer of 2010 to estimate θ across the DTS Transect (Figure 2.1a). Along with the DTS system the following continuously logging devices were also installed: 5 sets of observation wells with pressure transducers (HOBO U20 Water Level Data Logger, Onset Computer Corporation, Bourne, Massachusetts), 6 sets of dielectric θ sensors (5TM Soil Moisture and Temperature sensors, Decagon Devices Inc., Pullman, Washington) at depths of 10cm and 20cm, and 2 λ sensors (Thermal Conductivity sensors, East 30 Sensors, Pullman, Washington) (Figure 2.1a).

2.2.2. Estimating θ with Heated DTS

Estimating θ with heated DTS involves coupling temperature sensing with a resistance heating element. The heating element generates a heat pulse and the DTS system monitors the temperature within the cable using fiber optics. This temperature data is later processed to obtain ΔT from the onset of the heat pulse. ΔT is dependent on the θ of the surrounding soil. Dry conditions result in a higher ΔT in comparison to wet conditions because water helps bridge soil particles for improved heat transfer and provides a higher C_P (i.e. greater heat

storage potential). This dependency enables a DTS system coupled with resistive heating to also function as a distributed θ monitoring system.

The distributed θ monitoring system used in this study is described in detail by Striegl and Loheide (2012) and is comprised of the following components: a DTS system (Sensornet Ltd Halo DTS 4 km, BMP Enterprises, Houston, Texas), a custom designed fiber optic cable bundled with resistance heating wires and enclosed within a protective extrusion (Figure 2.2), a variable transformer (Variac 5021CT-2S, ISE, Inc., Cleveland, Ohio) for resistance heating power supply, and custom power control and timing instrumentation (GC 18SA120 and 7DT-2CH, ISE Inc., Cleveland, Ohio) to provide consistent timing, duration, and intensity of heating intervals. The DTS system transmits laser light down the fiber optics and records the backscattered light to determine the temperature of the cable at spatial resolution of 2 meters. A variable transformer is used to transform a 240 VAC input to an AC output ranging from 0 to 560 VAC to generate a heat pulse. The output from the variable transformer is controlled by the custom power control box and timing instrumentation, which can be programmed to change the timing and duration of heat pulses.

The cable was installed July 15, 2010 with a vibratory plow (DitchWitch 100SX vibratory plow) to knife the cable into the soil at a constant 20 cm depth and minimize soil disturbance. The DTS system estimates the average temperature of every 2 m section of the cable over the total 130 m length every 20 seconds. In 2010, the time between heat pulses was 4 hours, but this was changed to 2 hours in 2011. More details on the installation, calibration process, and technical aspect of this system can be found in previous studies (Striegl and Loheide, 2012; Striegl, 2011).

The ΔT metric for this study was defined as the difference between the average temperature from $380 \leq t \leq 580$ s after the onset of induced heating (T_{heat}) of 3.07 W/m and the ambient temperature (T_o). This metric will be referred to as $\Delta T_{8,}$ ($\Delta T_8 = T_{heat} - T_o$) because it represents the average ΔT around 8 minutes. Once ΔT_8 was determined, independently logging dielectric θ sensors located along the DTS cable were used to develop an empirical relationship between the observed soil moisture (θ_{obs}) and ΔT_8.

2.2.3. Modeling Contact Resistance and θ

A two-dimensional finite element method (FEM) numerical model of the cable cross section was created to simulate heat transfer away from the cable and into the surrounding soil during a 10 minute heat pulse. The FEM numerical model was created in COMSOL 4.3a with the two-dimensional Heat Transfer Module. The exact geometry of the cable cross-section (Figure 2.2) was obtained from the fabricator (Gulf Coast Downhold Technologies, Houston, Texas). The dimensions and thermal properties (density (ρ), C_P, and λ) of the cable components are shown in Table 2.1.

A thin thermally resistive layer was used to represent a contact resistance between the cable and soil. This layer is not explicitly represented in the model domain, but uses an effective layer thickness and layer λ (λ_{layer}) to calculate a thermal contact resistance between two domains (e.g. cable and soil). The thickness is divided by λ_{layer} to create a contact resistance in units of KW^{-1}. Representing this area around the cable as a contact resistance rather than an actual layer within the domain saves computational resources by avoiding the need to mesh a small gap between the cable and soil. To create this contact resistance, λ_{layer} was set to

the λ of air (0.025 W m^{-1} K^{-1}), and the thickness was varied from 0.01 to 0.8 mm. Subsequent plots express contact resistance both as a true contact resistance and as an air gap equivalence (AGE). Presenting the contact resistance as an AGE provides an intuitive means for conceptualizing the magnitude of the disturbed area, although a symmetric air gap around the cable is not physically realistic.

The thermal properties of the soil are dependent on θ, so a relationship between each thermal property and θ had to be developed to accurately model the cable under different θ conditions. C_P and ρ of the silt loam soil particles were estimated to be 870 J kg^{-1} K^{-1} and 2.3 g cm^{-3}, respectively (Ochsner et al., 2001). The porosity of the soil was known from multiple field samples. With the porosity, the proportion of air and water in the void space could be determined at any given θ, so the bulk C_P and ρ of the soil were estimated by summing the C_P and ρ of the soil particles, water, and air (de Vries, 1963). These calculations resulted in direct linear relationships with θ to input into the model.

The λ-θ relationship is not as straightforward because λ depends on heat flow paths, which are determined by the amount and orientation of water in the pore structure (Farouki, 1981). A λ-θ_{obs} relationship was developed by comparing field results from a dielectric θ sensor and λ sensor located at Location D (Figure 2.1). This relationship was developed using 12,673 points collected during the 2011 and 2012 growing seasons. A bi-exponential function was fit to the λ-θ_{obs} relationship using a least-squares regression (Figure 2.3). The coefficient of determination and root mean square error (RMSE) of the fitted function are 0.915 and 0.0547 W/m–K, respectively. These two sensors are separated by approximately 25 cm, so θ at these locations may not always be exactly equivalent, which may account for some of the scatter

about the λ and θ_{obs} relationship estimated by the fitted function. Hysteretic behavior between θ and λ may also explain some of the deviation from the primary relationship. Despite these sources of variability, the λ and θ_{obs} relationship was strong and used directly in our model. With C_P-θ, ρ-θ, λ-θ relationships, model simulations could be completed with different θ conditions.

Model simulations were completed for scenarios with and without a contact resistance. Adaptive computational time stepping was employed in COMSOL, with output recorded each second for the 600 second heating phase and 150 seconds of the cooling phase. The AGE was varied from 0.01 to 0.8 mm in 33 increments which were more tightly spaced on the low end of this range. For each contact resistance, θ of the surrounding soil was varied from 0.18 to 0.40. With a total of 34 contact resistance conditions (0 to 0.8 mm) and 23 θ conditions (0.18 to 0.40), 782 model simulations were completed. ΔT at the location of the fiber optics was averaged and saved from each simulation for comparison to the field data.

2.2.4. Estimating Contact Resistance from Field Data

As previously explained, ΔT is dependent on the contact resistance and θ. These two factors have a non-unique influence on ΔT. For example, an increase in ΔT could be a result of an increase in the contact resistance or a decrease in θ. This non-uniqueness makes it difficult to use ΔT from field data to estimate both contact resistance and θ. If the contact resistance could be monitored through time, then it may provide insight into the underlying mechanisms that cause contact resistances to develop. To predict the contact resistance, field data from the λ sensor at Location D was used to set the λ of the soil rather than using the λ-θ_{obs}

relationship developed in Figure 2.3; this choice guarantees that any hysteresis between λ-θ_{obs} of the soil (but not the disturbed zone represented by the contact resistance) is accounted for in the analysis. C_P and ρ of the soil were estimated using the method previously discussed, but the λ-θ_{obs} relationship was used to estimate θ from λ. Note that θ_{obs} could also have been used directly in this analysis and the results would not have been substantially different as there is a strong relationship between λ and θ_{obs}. Each heat pulse at Location D was compared to the model results for each contact resistance condition using the known λ from the λ sensor. A least square analysis was completed to determine which contact resistance parameterization best matched the field data from Location D.

2.3. Results

2.3.1. Transience in Contact Resistance: Impact on ΔT8

Increased contact resistance greatly increases ΔT within the cable above the expected response that occurs when the cable is in close contact with the soil (Figure 2.4). Simulated ΔT_8 values for the complete range of θ conditions were combined to produce relationships between ΔT_8 and θ for each contact resistance (Figure 2.5). As the contact resistance is increased, ΔT_8 also increases, but the shape of the ΔT_8 and θ relationship is similar for any given contact resistance. As previously noted, there is a non-unique relationship between the ΔT_8 and θ. An increase in ΔT may be a result of an increase in the contact resistance or a decrease in θ.

The least squares fitting analysis using field observed λ readings produced estimates of contact resistance (the only free variable) at Location D through time (Figure 2.6). A strong relationship between contact resistance and λ is evident; as λ decreases, contact resistance

tends to increase. A similar trend can be observed between contact resistance and θ_{obs}, which is expected as there is a strong relationship between λ and θ_{obs} (Figure 2.3). With variations in contact resistance seemingly correlated to λ and θ_{obs}, it is difficult to observe any temporal trends in the nature of the contact resistance independent of these hydrologically controlled fluctuations; that is to say, it is difficult to isolate changes related to the changing characteristics of the thermal connection between the sensor and the soil from changing thermal properties of the soil. To observe longer-term temporal trends, these same contact resistance predictions in Figure 2.6 were plotted against the corresponding θ_{obs} and grouped by year (Figure 2.7). The largest change in the relationship between contact resistance and θ_{obs} occurs between 2010 and 2011. There are much higher contact resistances in 2010 than in 2011 with similar variations in θ_{obs}. When comparing 2011 to 2012, there is a slight decrease in contact resistance during dry conditions. There appears to be no significant change between 2012 and 2013. Thus, the relationship between contact resistance and θ_{obs} appears to have asymptotically approached an equilibrium condition over a period of three years.

2.3.2. Hydrologically Driven Deviations from the $\Delta T8$ vs. θ Relationship

From September 20, 2010 to September 16, 2013, 8,027 heating pulses were initiated and recorded by the distributed θ monitoring system. Six dielectric θ and two λ sensors have logged concurrently for a majority of this time period. The relationship between ΔT_8 and θ_{obs} shows that this relationship is not stationary. To simplify the presentation, only data from Location D is displayed, but similar trends were observed for the other five locations and can

be found in Appendix A. Among the sites, there are differences in magnitude of these trends, but all locations show a consistent pattern. Location D was chosen from the six available locations because it had the least amount of θ_{obs} data gaps and was the location of the most complete λ dataset.

Major deviations from the primary relationship between ΔT_8 and θ_{obs} occur following wetting events after significant drying periods as illustrated using data from location D during the 2012 growing season (Figure 2.8). The soil is saturated at the beginning of this period and θ_{obs} ranged from 0.19 to 0.43 (Figure 2.8a). The first drying curve (Figure 2.8, b-1) shows a relationship between ΔT_8 and θ_{obs} similar in shape to that predicted in Figure 2.5. Following the first wetting event (b-2), ΔT_8 does not decrease to the extent expected for a substantial increase in soil moisture, but rather decreases only slightly, thus deviating from the initial drying curve (excursion to the right in b-2). The relationship realigns with the initial trend (b-1) after a long drying period (b-3). The wetting event following this long drying period (b-4) produces a drastic deviation from the initial drying curve. Again, θ_{obs} increases, but ΔT_8 only decreases slightly. Subsequent wetting events (b-5, b-6) shift the drying curve downward towards the initial (primary) drying curve. After a relatively long drying period (b-6), the curve returns approximately to the primary drying curve. Similar trends are observed in subsequent subplots (b-7 to b-11), each time showing excursion to the right of the primary drying curve. The last subplot (b-12) displays the largest wetting event of the growing season. The wetting curve follows the general trend of previous wetting curves following long drying periods, but it is reset to the beginning of the initial drying curve when near saturated conditions occur.

2.3.3. Long Term Trends in the ΔT_8 vs. θ_{obs} Relationship

In addition to the hydrologically-driven short term deviations in the relationship between ΔT_8 and θ_{obs}, long term trends were investigated using ΔT_8 data from the DTS cable at Location D that were paired with θ_{obs} data to analyze temporal changes between 2010, 2011, 2012, and 2013 (Figure 2.9). Drying curves that began at a point of near or complete saturation are highlighted to show data points unbiased by effects related to wetting events discussed previously. There are 27 points from 2010, 830 points from 2011, 1052 points from 2012, and 479 points from 2013 that were highlighted. These same periods are highlighted for the figures showing data from other locations in Appendix A.

It is not clear whether the selected drying curve from 2010 began at saturation, but it is the only extended drying period from this year and represents the time period immediately after installation. The first highlighted section from 2011 dries from saturation, but does not reach extremely dry conditions. There was a relatively complete drying curve later in 2011, but the DTS system was only collecting data during the driest section of the curve. These 2 sections of drying curves were combined to represent data minimally affected by wetting events in 2011. A similar process was completed for 2012 and 2013.

The largest shift in the relationship between ΔT_8 and θ_{obs} occurred between 2010 and 2011 with a significant decrease in ΔT_8 for all comparable θ_{obs} points (0.21 to 0.25). There is a slight decrease in ΔT_8 from 2011 to 2012, which occurs at θ_{obs} below 0.23. From 2012 to 2013, there appears to be no substantial change.

2.4. Discussion

The observation of hydrologically-driven shifts to the right of the typical $\Delta T_8 - \theta$ relationship following wetting events suggests contact resistance may be dependent on the previous wetting and drying cycles rather than being solely dependent on θ. In other words, the thermal response recorded by the DTS cable shows a hysteretic relationship with θ_{obs}. The second observation is a gradual decrease in ΔT_8 for a given θ_{obs} through time especially at low θ_{obs}. This trend is consistent with the soil becoming in better contact with the DTS cable as the soil structure heals following the initial installation of the cable.

2.4.1. Thermal Hysteresis

Thermal hysteresis in soils is a result of differing distributions of water in the pore structure. The thermal hysteresis in this field deployed DTS cable appears to be predominately related to the pore structure directly surrounding the cable rather than strong hysteresis in undisturbed soil. The pore structure between the cable and soil is likely different than the pore structure within undisturbed soil. This interpretation is supported by the independently logging λ sensor, which shows minimal hysteresis whereas the DTS, which has a similar theoretical foundation, shows strong hysteresis.

Physically, thermal hysteresis may be a result of pore water distributions surrounding the cable differing depending on the hydrologic history, soil shrinkage as the soil dries, or a combination of these two mechanisms. The pore distribution directly around the cable may not match the normal pore distribution of the soil farther from the cable. It would be expected that the pore distribution around the cable contains a greater frequency of larger pores as this soil was disturbed during the installation process. While these pores are large, they may not

be well connected with network of large pores typically responsible for infiltration in the undisturbed soil, and thus may not fill during wetting events. Small pores are important for heat transfer because small pores hold water longer into the drying process and essentially 'bridge' soil particles to one another or bridge soil particles to the cable. These bridges allow for efficient heat transfer. When a soil is dried, water first leaves the larger pores until only the smallest pores still contain water. Consequently, drying will minimize contact resistance for a given θ. For example, a soil that has been dried to a low θ will have water only in the smallest pores. If this soil is wetted, then water will first fill the empty, large pores because water most easily percolates through these pores. This increase in θ will only decrease contact resistance slightly because water located in a few large pores will not bridge as many soil particles as the same volume of soil would bridge if located in many small pores. Furthermore, the water flowing through the network of large pores in the soil may or may not be well connected to the network of disturbed pores surrounding the cable. This mechanism may explain the finding from Figure 2.7 where contact resistance seemed to be greater at lower θ. Another possible explanation for this θ-dependent contact resistance is soil shrinkage during drying. Shrinkage pulls individual soil particles closer together, which may cause the soil to pull away from the cable during drying. This mechanism would also introduce air gaps or a greater frequency of large pores directly around the cable. This gap may not swell reversibly as a result of wetting events that do not reach saturation. This process is analogous to our modeling approach, where the AGE thickness is used to represent the contact resistance to heat transfer from the cable to the soil matrix.

As seen in Figure 2.8, the first drying curve that starts at saturation (i.e. the primary drying curve) has the minimum contact resistance for any given θ_{obs}. When a wetting event occurs and the data shifts to the right of the initial curve, the following drying curve then moves back toward the initial $\Delta T_8 - \theta_{obs}$ relationship. This recovery trend observed after wetting events may be explained by water being depleted directly from the large pores that have little effect on soil λ or by water redistributing into smaller pores over time. When there is a long enough drying period, the $\Delta T_8 - \theta_{obs}$ relationship returns to the initial drying curve, which suggests the water in the disturbed soil near the cable is distributed in a similar fashion as it was prior to the wetting event. This distribution of pore water results in the minimum contact resistance for a given θ. The largest wetting event of the sample period shows an event that ends with the $\Delta T_8 - \theta_{obs}$ relationship returning to the beginning of the initial drying curve. At this point, the soil matrix is completely saturated – a state which must lay on the primary drying curve since there is only one possible distribution of pore water. The observed hysteresis may be quantifiable with a model that incorporates all scanning curves, but it would be complex and difficult to parameterize. Also, each relationship would be unique to the cable properties, soil type, and the age of the installation.

2.4.2. Soil Structure Healing

The contact resistance between the cable and soil appears to be getting smaller through time (Figure 2.9), with the largest change occurring between 2010 and 2011. This trend is consistent with a large initial healing or settling of the soil into any void space around the cable after installation. This gap between the cable and soil could be classified as pore space. When the soil water tension becomes large enough, water is withdrawn from this pore space.

The smaller this pore becomes, the larger the soil water tension will be required to withdraw the water. Realistically, there is a distribution of pore sizes between the cable and soil. To obtain a system with a minimal contact resistance, the pore distribution between the cable and soil must be similar to the pore distribution within the soil, a condition which becomes more likely as the disturbance heals. In 2010, there were likely many large pores between the cable and soil, but as the soil healed, these pores became smaller. There does not appear to be large differences between 2011 and 2012 except during the driest conditions. This suggests the pore distribution around the cable is still changing, but only the smaller pores that lose water at $\theta_{obs} \leq 0.23$ are becoming more numerous. As smaller pores become more numerous, more water is available to bridge the cable and soil particles, contributing to more efficient heat transfer. An increase in the efficiency of heat transfer results in a lower ΔT_8 within the cable. This transient relationship creates a difficult obstacle to estimating θ_{obs} from ΔT_8. This data also suggests that the soil structure surrounding the cable had not reached steady state conditions even two years after installation, but appears to be approaching steady state conditions after three years as 2012 does not differ significantly from 2013. Also, Location D appears to be approaching model results of no contact resistance, but several of the other locations are not as close to these model results as Location D, indicating that the rate of healing is spatially variable. This healing process is likely sensitive to the soil type and θ regime. Although the soil along this transect is consistently a silt loam, there are likely small variations in soil properties that may have varying effects on the healing process. It will be important in the future to compare these results to other field-deployed DTS systems in a

variety of environments to determine the length of time after installation to expect a time-dependent contact resistance due to soil healing.

2.4.3. Contact Resistance

The primary driver of transience in contact resistance between the cable and soil seems to be θ (Figure 2.6), which is intuitive since θ is the primary driver of temporal changes to λ in the soil. The previously discussed thermal hysteresis and soil structure healing are both issues related to the interface between the cable and soil and can be quantified with a contact resistance. The thermal hysteresis adds hydrologically driven behavior to the contact resistance – θ relationship, and the soil structure healing adds a long-term, time-dependency to the contact resistance – θ relationship. Figure 2.9 suggests that Location D may no longer be changing through time, but the other five locations appear to have not yet reached a stable condition. The obstacles to using heated DTS systems to estimate θ identified in this study (thermal hysteresis, soil structure healing, soil shrinkage, and spatial heterogeneity) each seem to be related to contact resistance. It is conceivable that the relationship between contact resistance and θ could be parameterized and later taken into account when estimating θ from the DTS system. However, this relationship would be difficult to determine due to its transience and high spatial variability, and thus, may not be the best path forward in developing improved methods for analyzing DTS data for estimating θ.

Although contact resistance and θ have a non-unique influence on ΔT_8, these two variables affect the heating and cooling phase of a heat pulse differently. Contact resistance affects early time sections of heating and cooling phases whereas θ affects late time sections of heating and cooling phases. In theory, a sufficiently long heat pulse can predict contact

resistance and θ, but it would require more sophisticated methods than using a single metric such as ΔT_8. Preliminary analysis indicates that low signal to noise ratios may hamper efforts to pursue analysis of late time data where temperature changes are small and slow with the experimental set-up tested here.

2.5. Conclusion

Data collected from a field deployed heated DTS cable for approximately three years led to the observation of soil thermal hysteresis in the disturbed zone near the cable and soil structure healing. Both of these phenomena are caused by air gaps that create a contact resistance between the cable and soil. Model simulations with and without a contact resistance between the cable and soil provided an opportunity to observe the effect of contact resistance and θ on ΔT during a heat pulse. These simulations showed that contact resistance and θ have a non-unique influence on ΔT_8. This finding suggests contact resistance must be known before θ can be estimated.

The model simulations also allowed for comparison to field results at select points along the transect where independently logging sensors were located to estimate the magnitude of contact resistance both qualitatively (Figure 2.9) and quantitatively (Figure 2.6). These comparisons led to the finding of a strong relationship between contact resistance and θ. Contact resistance is minimized in near saturated conditions and maximized in dry conditions. In theory, this relationship could be used when analyzing ΔT from a heat pulse to estimate θ, but the contact resistance – θ. relationship is complicated by thermal hysteresis, time-dependency (i.e. soil structure healing), and spatial heterogeneity. With this complex

relationship and the previously discussed non-uniqueness between contact resistance and θ, estimating θ from a single metric such as ΔT_8 may not be possible. There may be opportunities to develop new, or use existing, more sophisticated methods of analyzing heating and cooling phases from a heat pulse, which either circumvents the need to estimate contact resistance or is capable of estimating contact resistance and θ from a single heat pulse.

Acknowledgements

This material is based on work supported by the National Science Foundation under Grant CBET- 0954499. Any opinions, findings, conclusions, or recommendations expressed in this material are those of the author(s) and do not necessarily reflect the views of the funding agencies. We would like to thank Arlen Striegl for his initial design and development of this DTS system, as well as the following individuals for helpful discussions and/or logistical field support during the research effort: Eric Booth, Eric Mark, Matt Weber, and Carolyn Voter.

Tables & Figures

Table 2.1. Dimensions and thermal properties of principle components of heated DTS cable.

Component Number	Cable Component	Diameter (mm)	Radius (mm)	Thermal Conductivity (W/m-K)	Heat Capacity (J/kg-K)	Density (kg/m^3)
1	Fibers within stainless steel capillary tube (4)	0.05	0.025	1.38	740	2200
2	Sepigel lubrication around fibers	1.067	2.134	0.14	1560	850
3	Stainless steel capillary tube	1.321	2.642	16	500	7916
4	Nichrome wire	0.511	1.021	13.3	435	840
5	Copper wire	0.511	1.021	401	385	8940
6	PFA Insulation	1.321	2.642	0.195	1172	2150
7	Nylon 6 Filler Rods	3.963	7.926	0.25	1310	1130
8	Polypropylene tape wrap	4.117	8.233	0.113	1900	900
9	Polypropylene extrusion	7.367	14.733	0.113	1900	900

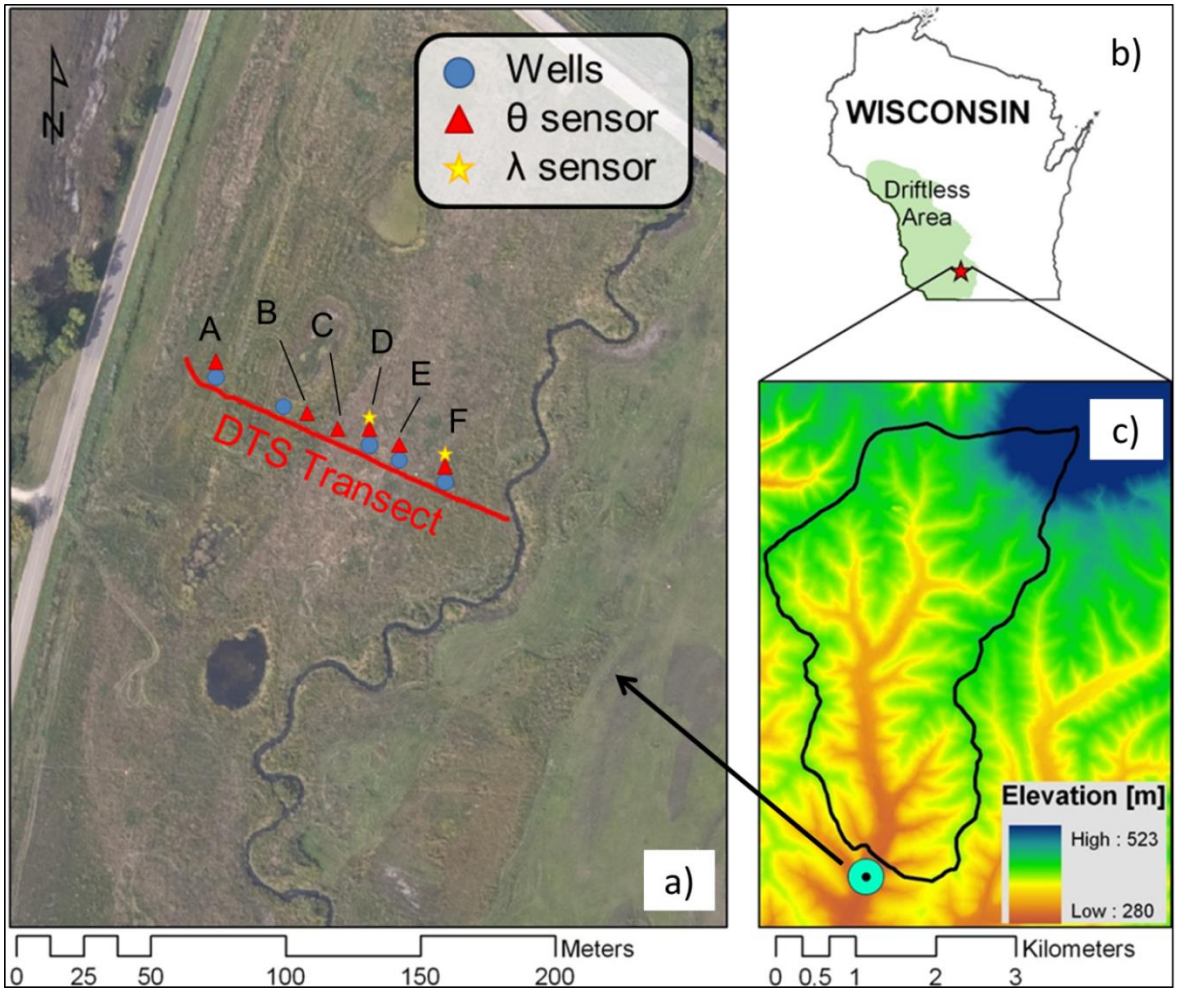

Fig. 2.1: The field site is located in southwest Wisconsin (b) south of the East Branch Pecatonica River Watershed displayed in the digital elevation model (c). The DTS Transect is located along the red line with observation wells (blue circles), dielectric θ sensors (red triangles), and λ sensors (yellow stars) with labels assigned to each dielectric θ sensor (a).

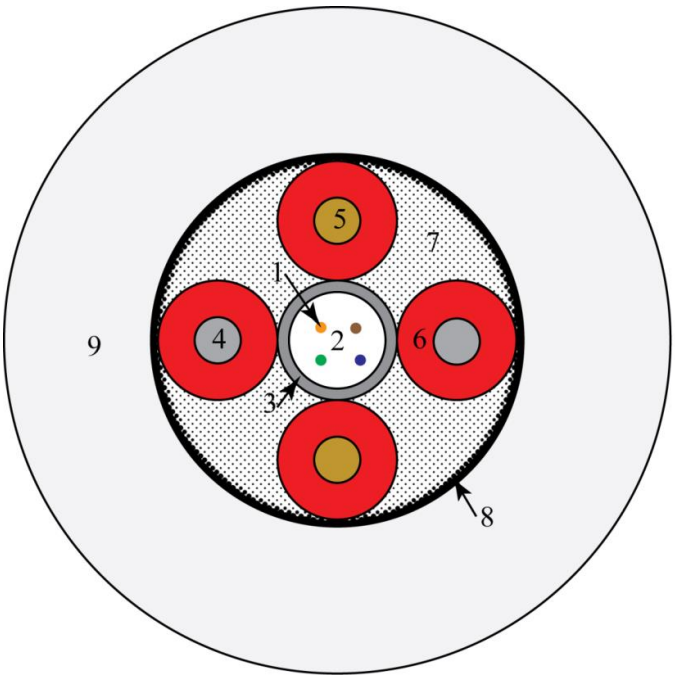

1. 50 µm fiber optics (x4)
2. Sepigel lubricant
3. 1.32 mm stainless steel capillary tube
4. 0.51 mm NiChrome resistance heating wires (x2)
5. 0.51 mm copper wires (x2)
6. 1.32 mm PFA wire insulation (x4)
7. Nylon filler rods
8. 4.12 mm polypropylene tape wrap
9. 7.37 mm polypropylene extrusion

Fig. 2.2: Heated DTS cable cross section with overall diameter of 7.37 mm.

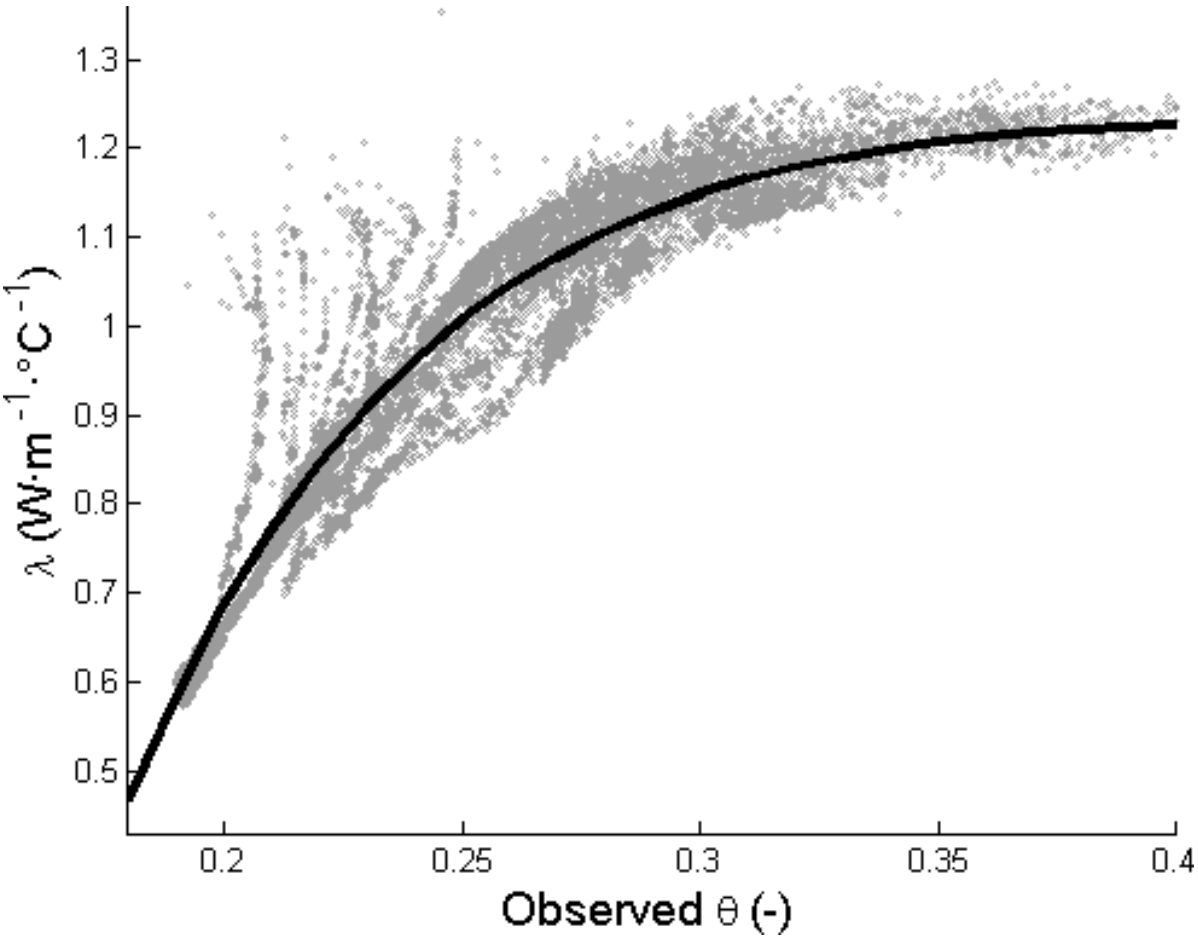

Fig. 2.3: A bi-exponential function was fit to data from a dielectric θ sensor and λ sensor co-located at Location D. This regression was used to estimate λ for θ ranging from 0.18 to 0.40.

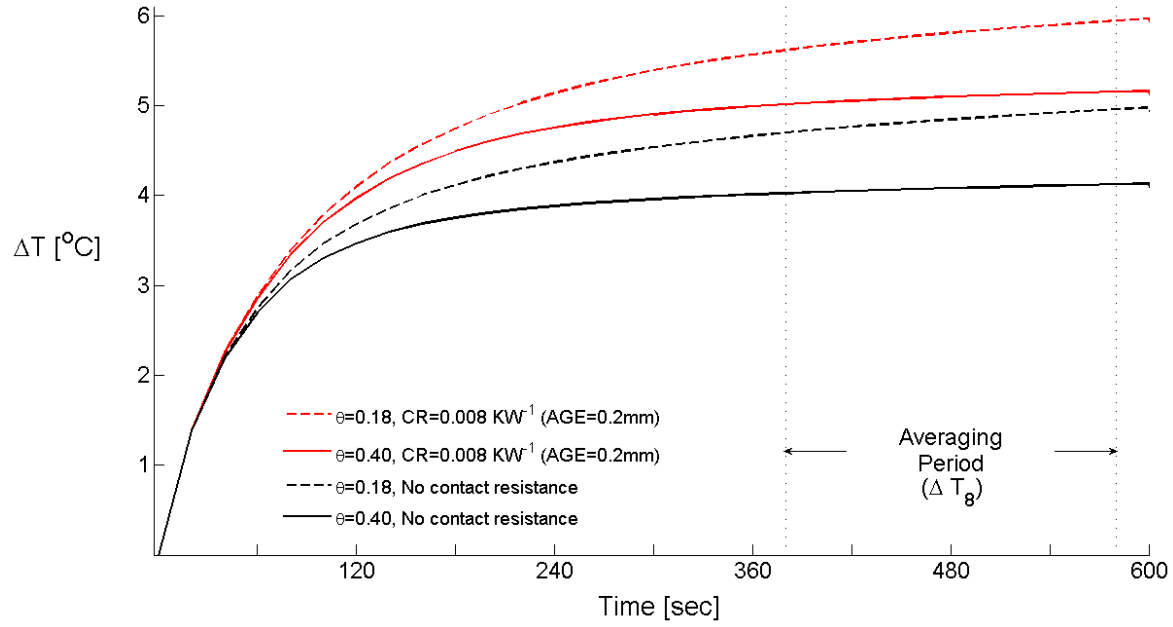

Fig. 2.4: Model results of the temperature response at the center of the cable during a 10 minute heat pulse under two θ conditions (0.18 represented by solid lines and 0.40 by dashed lines) and two contact resistance conditions (no contact resistance in black and 0.2mm contact resistance in red).

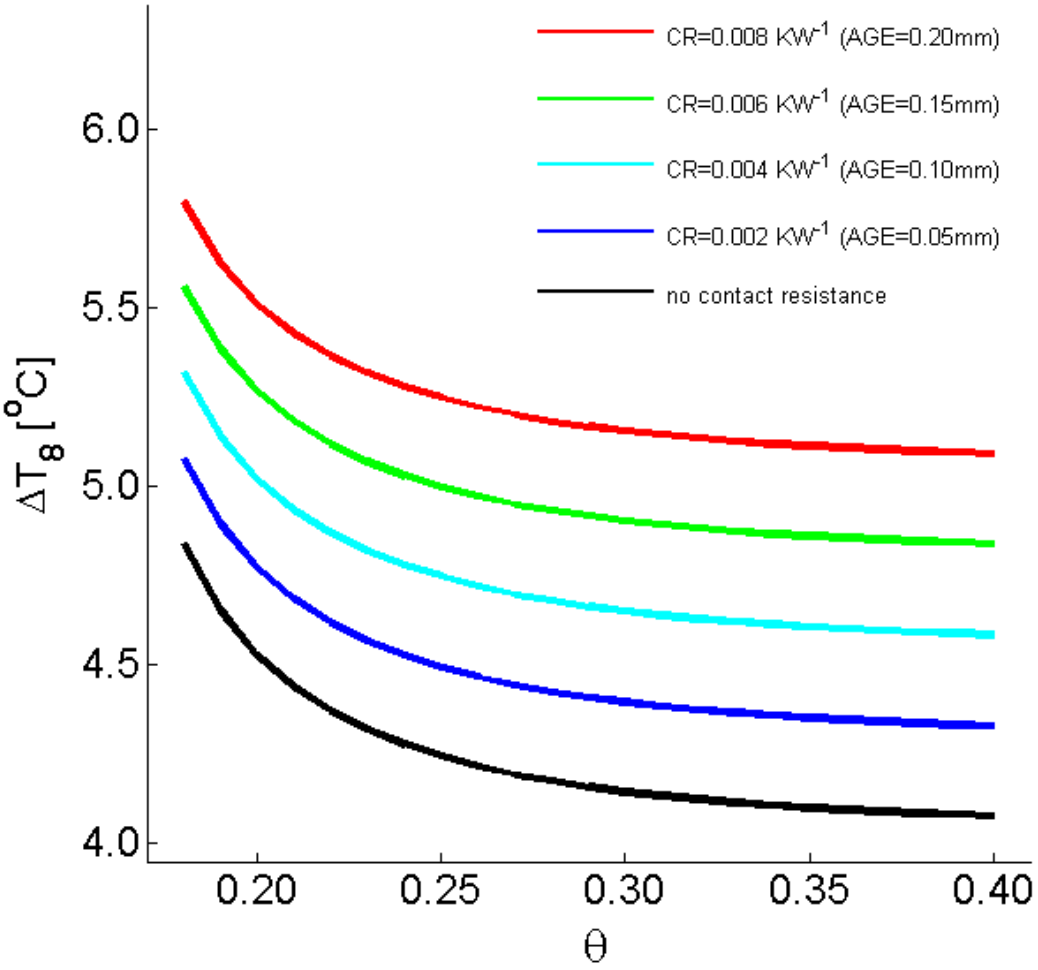

Fig. 2.5: Model results of ΔT_8 at 23 θ conditions for 5 contact resistance conditions. No contact resistance is shown in black, a contact resistance of 0.002 KW^{-1} is shown in blue, 0.004 KW^{-1} in cyan, 0.006 KW^{-1} in green, and 0.008 KW^{-1} in red.

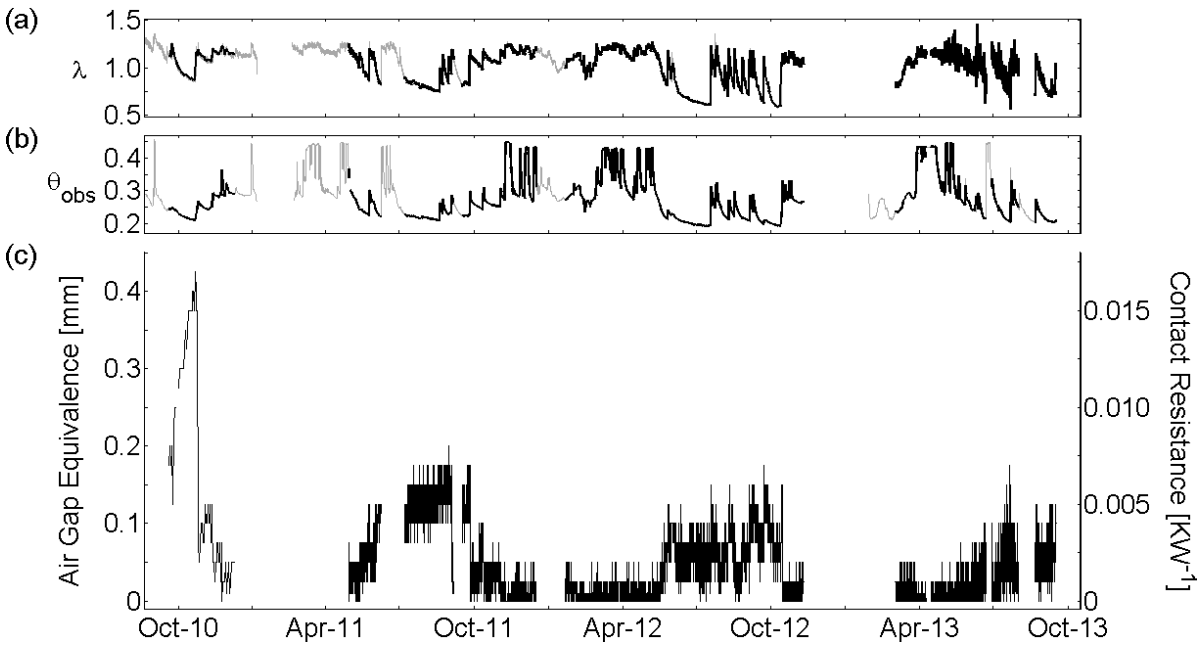

Fig. 2.6: λ data (a) from a λ sensor at Location D were used to predict contact resistance along the DTS cable at Location D (c). Data from a dielectric θ sensor are shown for comparison (b). Bolded sections of (a) and (b) represent time periods when DTS data was collected.

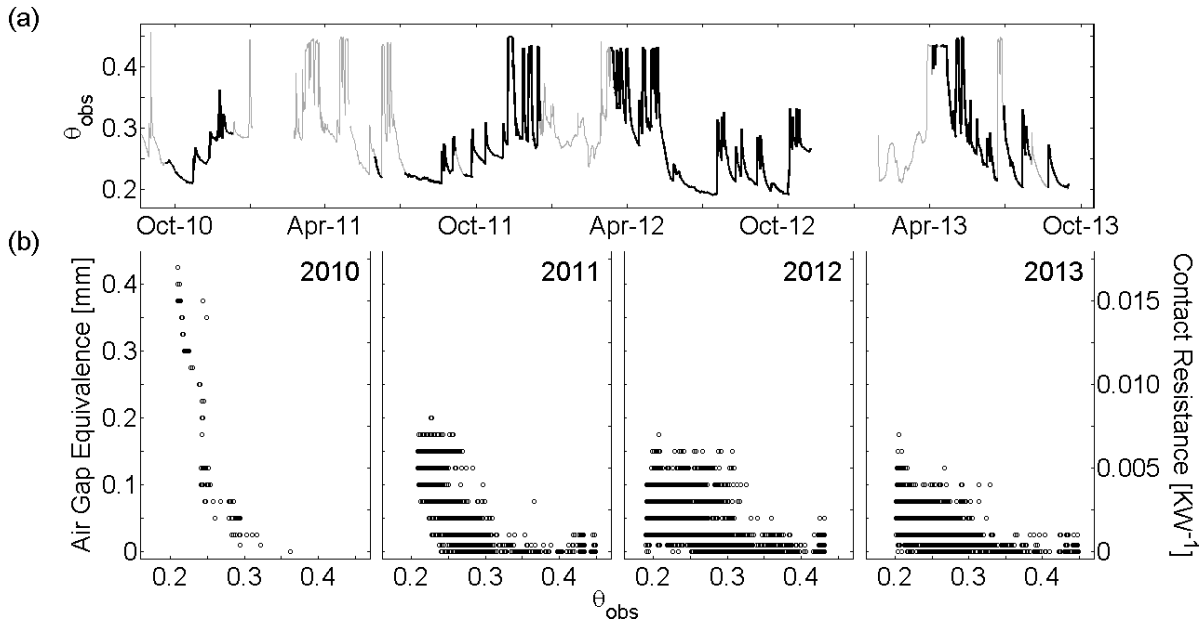

Fig. 2.7: Dielectric θ data from Location D are shown in (a). Bolded sections represent periods when DTS data was collected. (b) shows the contact resistance predictions from Figure 2.6, but plotted versus the corresponding θ reading from (a). Data is grouped by year to observe temporal trends in the contact resistance to θ relationship.

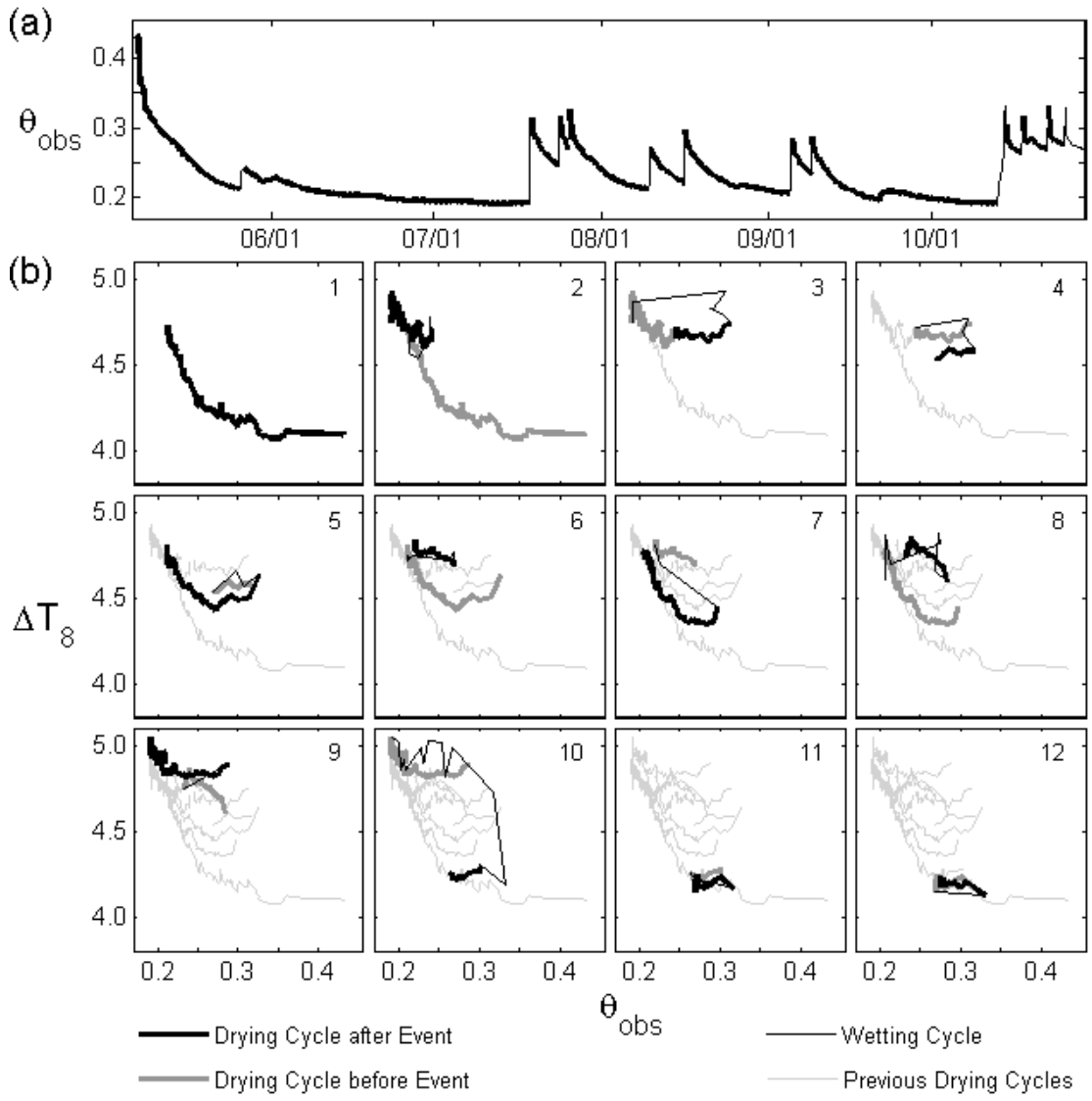

Fig. 2.8: (a) shows the θ time series from a dielectric θ sensor located at Location D along the DTS cable. (b) shows the corresponding ΔT_8 response (13 point moving average) at this location on the DTS cable versus the θ_{obs} graphed in (a). Each separate subplot within (b) represents a different wetting event (except for b-1, which displays the initial drying curve). Subplots display the drying curves prior to the wetting event in gray, wetting curves with a thin black line, drying curves following the wetting event in black, and all previous drying curves with thin gray lines.

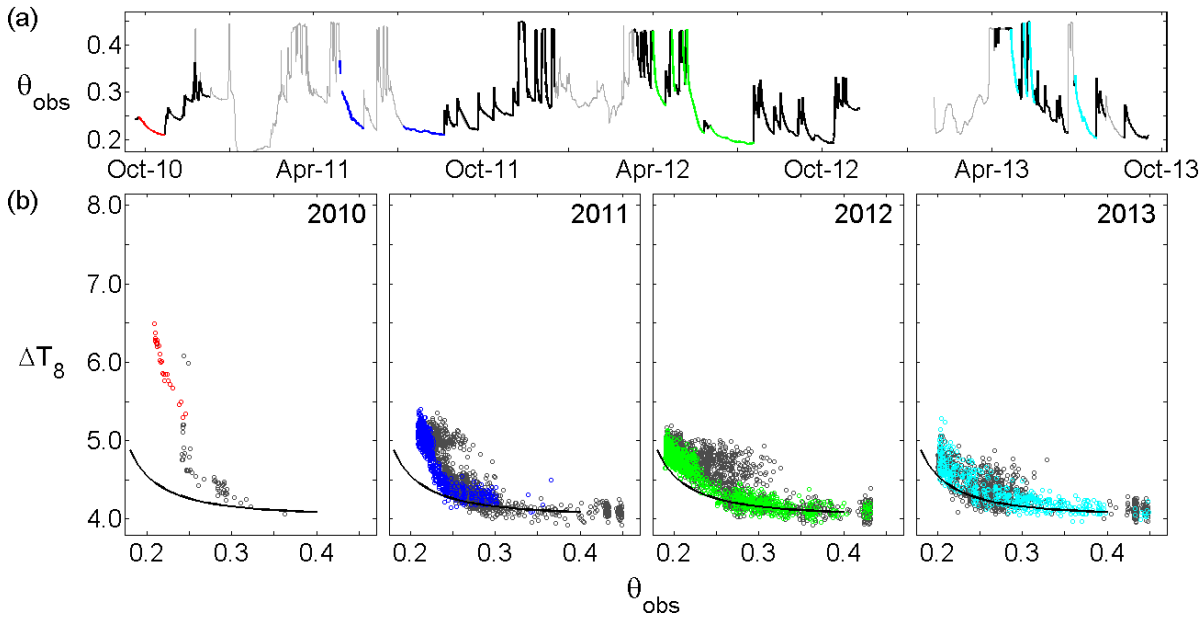

Fig. 2.9: Data from a dielectric θ sensor located at Location D from September 2010 to September 2013 (a). Bold and colored sections represent data that have corresponding DTS data for that time period. Colored sections were highlighted because DTS data is available at those dates and these sections have dried from near saturation without any significant wetting events prior. These time periods are minimally affected by soil thermal hysteresis. These sections have been grouped by year: 2010 (red), 2011 (blue), 2012 (green), and 2013 (turquoise). θ_{obs} data are paired with ΔT_8 data from the section of the DTS cable where this dielectric θ sensor is located (b). Time periods highlighted in (a) are also highlighted in (b). Remaining DTS data in bold sections in (a) are displayed in gray in (b).

Chapter 3: Proposed data processing approaches for estimating soil moisture with heated distributed temperature sensing

University of Wisconsin –Madison

Madison, Wisconsin

3.1. Introduction

Heated distributed temperature sensing (DTS) is an emerging technology with the potential to estimate soil thermal properties across distances greater than 10 km, spatial resolutions less than 2 m, and temporal resolutions less than 4 hours (Sayde et al., 2010). Soil thermal properties, such as thermal conductivity (λ) and heat capacity (C_P), are strongly dependent on the soil moisture (θ) (Shiozawa and Campbell, 1990), which allows θ to also be estimated from these heated DTS systems. An instrument that can provide θ estimates across spatial and temporal scales could be used for a wide range of applications such as flood forecasting, precision agriculture, and understanding complex ecological processes (Ochsner et al., 2013).

The general concept behind heated DTS systems is similar to conventional heat pulse sensors, which are typically point sensors rather than spatially distributed sensors. There are two general types of heat pulse sensors: single and dual probe. The heat source and temperature observations are colocated in single probe sensors, whereas dual probe sensors make temperature observations at a distance from the heat source. Single probe sensors typically consist of a stainless steel capillary tube, resistance heating wires contained within the capillary tube, and a thermistor set in the center of the probe. A constant heat source is applied to the heating wires for a given duration to generate a heat pulse. The temperature response is monitored by the thermistor. The rate of the temperature response and the maximum temperature response are dependent on λ of the surrounding medium. The advantage to dual probe sensors is the capability to estimate both λ and C_P, whereas single probe sensors can only estimate λ (Bristow et al., 1994). Most heated DTS systems have been

designed to have the temperature sensing fiber optics and heat source located in the same cable, so these cables function similarly to single probe heat pulse sensors.

The largest differences between heated DTS systems and conventional single probe sensors are probe length and size (i.e. cross sectional area). Conventional single probe sensors are shorter in length because they are point sensors whereas DTS systems are spatially distributed. DTS systems also have larger diameters because the fiber optic cables occupy more space and DTS cables are often covered or coated with material to hold the components together and provide environmental protection. This layer of protection is considered necessary as replacing a damaged cable would be expensive and time consuming. Protective layers are not common with single probe sensors as these sensors are relatively cheap and easy to replace. An added layer increases the response related solely to the cable properties and reduces the duration that the temperature response is primarily dependent on the soil properties. DTS systems use a higher power input and a longer heating duration to overcome this disadvantage of a larger diameter. The installation process is also much more invasive for DTS cables. A DTS cable requires a trench to be dug to bury the cable or a plow to knife the cable into the ground. Single probe sensors can be gently pushed into undisturbed soil after digging a hole adjacent to the area of interest. Consequently, DTS cables are expected to exhibit poorer thermal contact with the surrounding soil, which can be expressed as a higher thermal contact resistance. Thermal contact resistance is the total thermal resistance to heat flow between two objects. The magnitude of the contact resistance in DTS cables may be larger due to the larger size. For these reasons, DTS cables will likely require consideration of their finite radius and contact resistances, which will be discussed after a

general discussion of conventional methods to interpret the temperature response of single probe sensors.

There have been several techniques used to interpret the temperature response of a single probe heat pulse into λ, but most focus on aspects of the analytical solutions. Analytical solutions have been developed for infinite line sources (de Vries, 1952) and infinite cylindrical sources (de Vries and Peck, 1958) of constant heat. From these solutions, the temperature response is found to vary linearly with log time. λ can be calculated from the slope of the best fit line if the heating current and heating wire resistance are known (de Vries and Peck, 1958; Shiozawa and Campbell, 1990). This linear aspect of the analytical solutions allows for graphical estimations of λ or nonlinear regressions to estimate λ.

It is desirable to design small probes as smaller probes will minimally disturb the soil, have less influence from their finite radius on the temperature response, be less influenced by contact resistances, and require less heat (Weiss, 2003). Contact resistances and the finite radius of probes require time corrections or the use of only late time data to estimate λ (de Vries, 1952; Shiozawa and Campbell, 1990; Weiss, 2003). Weiss (2003) showed that the use of late time data approximates the properties of the surrounding soil despite the presence of a finite probe and contact resistance. This finding is especially important for DTS systems as the DTS cable is much larger than conventional λ sensors, so the use of late time data will be necessary.

To convert λ to θ, an additional step is necessary. Many studies have used λ estimates to infer θ using a calibration equation (Chung and Horton, 1987; Mortensen et al., 2006; Weiss, 2003). Some studies have tried to simplify the data interpretation process by avoiding the need to estimate λ and simply correlating the maximum temperature response to θ (Shaw and Baver, 1940; Striegl and Loheide, 2012; Youngs, 1956). Weiss (2003) used a heated DTS system to estimate λ using the late time approximation of the analytical solution discussed by Shiowaza and Campbell (1990) and then inferring θ using a calibration equation. Weiss (2003) was able to differentiate between wet and dry soils, but the slope of the late time data did not vary significantly for $\theta > 0.06$. Also, noise inherent with DTS systems caused inaccuracies. Developments have been made with more current DTS systems to reduce this noise, but the finding of this early study on heated DTS systems led researchers to pursue other data interpretation techniques. Sayde et al. (2010) incorporated the entire temperature response curve by integrating the temperature response through time to get a cumulative temperature response metric (T_{cum}). Striegl and Loheide (2012) defined a maximum temperature response metric (ΔT_8) by averaging late time data. Both of these studies then correlated these metrics to θ to create calibration curves. These two data interpretation techniques found a similar trend to Weiss (2003) where the sensitivity of the calibration curves decreased as θ increased, but these two techniques did appear to be more sensitive than the method used by Weiss (2003). This increased sensitivity is likely a result of a θ-dependent contact resistance that increases as θ decreases. An increase in the contact resistance will increase the temperature response within the cable. Typically, contact

resistances will increase as θ decreases as was seen in Chapter 2, which may explain the greater sensitivity.

The issue that may arise using either of these two techniques is a θ-dependent contact resistance that changes through space or time. In Chapter 2, it was found that contact resistance is strongly dependent on θ, but other factors were also found to affect the contact resistance. The magnitude of the contact resistance decreased through time as the soil structure healed following the cable installation. Also, the contact resistance was dependent on the previous wetting and drying cycles. All these dependencies must also not vary through space for the calibration curve to be applied across the length of the cable. Since contact resistances can vary for a given θ, there is a non-unique relationship between the T_{cum} and ΔT_8 metrics and θ, but the slope of the temperature response at late time using by Weiss (2003) is theoretically not dependent on the contact resistance if the heat pulse is sufficiently long to be unaffected by the cable properties and contact resistance.

The objective of this chapter is to develop and evaluate alternative data processing techniques to estimating θ from a heated DTS system assuming that contact resistances are not temporally constant or do not vary monotonically with θ. The proposed methods will be assessed using synthetic data sets representing the temperature response from a heat pulse under different θ and contact resistance conditions.

3.2. Methods

3.2.1. Heated DTS System & Cable Design

The two primary components of the heated DTS system are a DTS processor and a custom-made cable. The custom-made cable is comprised of 4 fiber optic cables bundled with heating elements. The outside of this cable is coated with polypropylene to provide protection from the elements. The power for each heat pulse is transformed from a 240 VAC input to a 560 VAC output, which generates 3.07 Wm^{-1}.

The following model is based on the heated DTS system discussed in Chapter 2. A DTS processor and custom-made cable are used. The cable is a fiber optic bundle coupled with resistive heating (Figure 2.2). The fiber optics are located in the center of the cable and are surrounded by four heating elements, which generate the heat pulse. The power input to generate the heat pulse is 3.07 Wm^{-1}. These components are protected by a polypropylene extrusion, which brings the diameter of the cable cross section to 7.37 mm. The timing and duration of each heat pulse is controlled by a timing mechanism, and the power input can be manually changed with a variable transformer. All of these devices are housed in an environmentally controlled structure. A heating and air conditioning unit provides a relatively constant ambient temperature within the shed.

3.2.2. 2D Transient Finite Element Model

The two-dimensional finite element method (FEM) numerical model of the cable cross section used in Chapter 2 was altered to model the temperature response at 20-second intervals for a 60-minute heat pulse and a subsequent 60-minute cooling phase. The heat pulse was changed from 10 minutes to 60 minutes to gain a better understanding of the effect

of contact resistance and θ on late time data. Early time data is strongly influenced by cable properties with contact resistances having a strong influence on early to mid-time data. The length of the cooling phase was extended to determine whether it could provide information related to contact resistances or θ. The time interval was changed to provide an interval that would be more realistic to actual data from a DTS system as the recommended minimum interval is 10 seconds to reduce noise. Inherent noise could be reduced (i.e. temperature resolution improved) in real DTS systems by increasing this interval. The DTS system being modeled currently obtains temperature readings every 20 seconds because two 10 second readings are taken with the double ended measurement technique, so the time interval used with this model was 20 seconds.

Model simulations were completed for conditions with and without a contact resistance. To gain a better perspective on the magnitude of this contact resistance, the equivalent air gap between the cable and soil to produce each contact resistance was calculated. This conversion allows the contact resistance to be reported in units of resistance and an air gap equivalent (AGE) thickness. The contact resistance was varied from 0.01 to 0.8 mm in AGE in 32 increments. For each contact resistance condition, θ of the surrounding soil was varied from 0.18 to 0.40 using the same methods from the previous chapter. With a total of 33 contact resistance conditions (0 to 0.8 mm) and 23 θ conditions (0.18 to 0.40), 759 model simulations were completed. ΔT from the location of the fiber optics was averaged and saved from each simulation to create a synthetic temperature response. To assess the robustness of each processing technique, synthetic, random noise was introduced to the model results. A

random error with a normal distribution and a standard deviation of 0.05°C was introduced to each temperature reading. These synthetic model results with noise were then processed using the two data processing techniques outlined below to determine which approach provided more accurate θ estimates with the presence of random noise. This analysis was repeated with a standard deviation of 0.005°C.

3.3. Results

Two data processing approaches were found to be capable of estimating θ despite the presence of a contact resistance. The first method involves parameterizing the contact resistance prior to estimating θ. The second method involves estimating θ independently of the contact resistance using late time data similar to the method used by Weiss (2003). Both methods require non-linear regression approaches as the temperature response does not vary linearly through time (Figure 3.1).

3.3.1. Estimating θ after Parameterizing Contact Resistance

Contact resistance appears to affect the temperature response before θ has any significant effect at early time (Figure 3.2). This observation suggests early time data could be used to parameterize the contact resistance from each heat pulse, regardless of θ conditions. To fit a linear function through the non-linear, early time data, the temperature response was plotted against the logarithm of time (Figure 3.3). The fitting period used was 40 to 120 seconds as contact resistance had a minimal effect on the temperature response before 40 seconds, and after 120 seconds, θ began to have a more significant effect. A line was fit to this early time data for each simulation and the results for the two extreme θ conditions show the influence

of θ on the slope of this line (Figure 3.4). The slope of this fit is more influenced by θ at lower contact resistances than at higher contact resistances.

The contact resistance could also be estimated by analyzing the cooling phase of the heat pulse. The early time data from the cooling phase has the same characteristics of the heating phase. Very early time data is largely controlled by the cable design. Shortly after this time period, contact resistance largely affects the slope of temperature response against the logarithm of time, and late time data is largely controlled by θ. A similar regressive analysis that was used to estimate contact resistance from the heating phase can be completed on the cooling phase. ΔT can be plotted against the logarithm of time after heating ended. The slope of this relationship can be used to approximate the contact resistance, but the appropriate fitting period must first be identified. The period that appears to be most dependent on the contact resistance and minimally affected by θ is 60 to 140 seconds after the onset of the cooling phase (Figure 3.5). The slope of the best linear fit within this fitting period was determined for each model simulation. To observe the impact that θ has on this slope, the two θ conditions extremes (0.18 and 0.40) were plotted (Figure 3.6). All other θ conditions were estimated to be points between these two lines. Similar to Figure 3.4, θ has a larger impact at lower contact resistances.

Once the contact resistance is estimated from the average of the estimates obtained from the early time heating phase and early time cooling phase analyses, then a single metric describing the maximum temperature response could be used to estimate θ as each θ condition has a unique maximum temperature response for a given contact resistance (Figure

3.7). The maximum temperature response metric that will be used as an example is the average temperature during the final 10 minutes of the heating phase (ΔT_{55}). This metric is a similar metric to ΔT_8, which was used in the previous chapter. Once the contact resistance is known, a calibration relationship can be simulated by taking all the ΔT_{55} values from Figure 3.7 and plotting versus θ for each contact resistance condition (Figure 3.8). Once the contact resistance is estimated, then the appropriate curve can be selected from Figure 3.8 to determine θ.

3.3.2. Estimating θ with Late Time Data

Estimating θ independently of the contact resistance is also possible by analyzing the late time temperature response versus the logarithm of time. After a sufficiently long time, the relationship between the temperature response and the logarithm of time becomes linear and is primarily dependent on θ of the surrounding soil (Figure 3.9). The length of time before this log-linear behavior begins will be dependent on the cable properties and magnitude of the contact resistance. The fitting period used for this analysis was 40 to 60 minutes. Given the relationship in Figure 3.9, slopes determined from field data could be used to estimate θ. The slope of each simulation from Figure 3.9 was minimally affected by the contact resistance (Figure 3.10). Also, there is not a substantial difference in this slope at θ above approximately 0.30.

3.3.3 Error Propagation Analysis

Synthetic, random noise with a standard deviation of 0.05°C was added to all 759 model simulations to determine which method was least affected by the random noise associated with the accuracy of a Halo DTS system. These synthetic results were processed using the

two methods outlined above to determine estimates of θ. The median curve for Figure 3.4, 3.6, and 3.10 were chosen to create an empirical relationship between various parts of the temperature response curve. Two iterations were completed to generate two sets of 759 synthetic temperature response curves each with random noise. The first method that parameterized the contact resistance prior to estimating θ had a RMSE of 0.075 whereas the second method that used the late time slope of the temperature response had a RMSE of 0.082. Both methods were more accurate with dry conditions ($\theta < 0.30$) than wet conditions ($\theta \geq 0.30$), and the first method provided slightly more accurate estimates than the second method under both dry and wet conditions (Table 3.1).

All results of the error propagation analysis were plotted to observe the deviation from the model results (Figure 3.11). It is important to note the method that contact resistances were predicted with the first method. Once the empirically-derived contact resistance was determined from Figure 3.4 and 3.6, a calibration curve had to be chosen. These calibration curves were created for modeled intervals of contact resistance, so the nearest match to the empirically-derived contact resistance was used. This created some unusual patterns in Figure 3.11a-b, and may have artificially lowered the RMSE for this technique.

3.4. Discussion

3.4.1. θ Estimation after Parameterizing Contact Resistance

The error propagation analysis showed that estimating θ after parameterizing the contact resistance is a more robust method than estimating θ from the slope of the late time temperature against log time. This method depends on obtaining contact resistance estimates

from early time heating phase and early time cooling phase data, and then using these estimates to select a calibration curve that uses the late time data average (ΔT_{55}) to obtain θ. The error propagation analysis assumes that exact calibration curves have been created as these curves were created without noise, but in reality, these calibration curves may be difficult to create. Creating calibration curves for different contact resistances (i.e. varying slopes of early time temperature response against log time) would require a large amount of data across a range of conditions. These calibration curves could be created with an accurate model, but an accurate model would also likely require a large amount of data for validation purposes.

Beyond this potential difficulty, this method could be improved by obtaining better estimates of contact resistance. As a review, very early time data is mostly dependent on the cable design. Cables with smaller diameters and more thermally conductive materials will provide less data related to the cable design for a given induced heat pulse. Increasing the induced heat pulse will also decrease the time period where data is highly dependent on the cable design. The temperature response following this very early response is most affected by the contact resistance (if a contact resistance is present). As the heat pulse continues, the temperature response becomes more dependent on the properties of the surrounding medium. Similar to the cable design, the smaller the contact resistance and the larger the induced heat pulse, the shorter this period will be highly dependent on the contact resistance.

To accurately parameterize the contact resistance, it would be helpful to have several temperature response data points during the period where the temperature response is primarily dependent on the contact resistance. One way to increase the number of data points

is to reduce the intensity of the heat pulse. The tradeoff with reducing the intensity of the heat pulse is a longer period before the temperature response is primarily dependent on θ. A longer period would also be more prone to errors associated with ambient temperature drift, water movement, and vapor movement.

One potential method to increase the precision of the contact resistance parameterization is to generate several small heat pulses that would each provide an estimate of the contact resistance. These small heat pulses could be made prior to a long heat pulse. Additional modeling would be required to determine the optimum magnitude and duration of induced heating and the necessary time step required between pulses to insure subsequent pulses are not influenced by the heat generated from previous heat pulses.

Once the contact resistance is estimated, θ can be determined by analyzing the maximum temperature response metric (ΔT_{55}). It is important to note that the ΔT_{55} was used because data from a 60 minute heat pulse was available. Averaging the temperature response at an earlier period would also provide information about θ, but the calibration curves for higher contact resistances may be less sensitive to changes in θ. The calibration curves created for ΔT_{55} (Figure 3.7) show minimal influence from the contact resistance (i.e. each curve has a similar shape). There is not a strong signal for $\theta \geq 0.30$ (Figure 3.7 and 3.8). This finding is expected as λ_{soil} does not vary substantially for $\theta \geq 0.30$. This weak signal at higher θ is a drawback to using the single probe method (temperature sensing and heat source are colocated). Dual probe methods (temperature sensing some distance from the heat source)

are capable of estimating λ and heat capacity. Heat capacity varies linearly with θ, so it can be a better predictor of θ than λ.

3.4.2. θ Estimation Independent of Contact Resistance

Using the slope of the late time data to estimate θ has similar drawbacks to the previous method where there is less sensitivity at higher θ. The advantage to this method is the ability to estimate θ independent of the contact resistance. It is not necessary to parameterize the contact resistance or develop calibration curves for different contact resistance conditions. The disadvantage to this method is that it appears less accurate than the previous method with the introduction of noise, although the largest deviation appears to occur during wet conditions ($\theta \geq 0.30$), which is expectedly inaccurate for both methods. A longer heat pulse would provide more data to determine a more accurate slope. The drawback to increasing the duration of a heat pulse is the previously mentioned ambient temperature drift, water movement, and vapor movement.

3.4.3. Application of Results to Other Heated DTS Systems

These model results are specific to the magnitude and duration of the heat pulse, the cable design, and the soil properties, but the same trends should be expected across all heat pulse sensors. It may not be feasible to develop a model for each heated DTS system; it also may be difficult to develop a model that adequately matches field conditions. Although model results would be helpful to begin developing model generated calibration curves such as Figure 3.4, 3.6, 3.8, or 3.10, the more realistic application to these results is to inform the interpretation of collected data. There is not an easy method to measure the contact resistance, so it is not realistic to develop a field-informed calibration curve similar to Figure

3.4 or 3.6. However, there are relatively cheap and easy methods to measure θ (e.g. dielectic θ sensors), which could be used with some metric of contact resistance such as the early time slope to generate calibration curves similar to those in Figure 3.8. The contact resistance would not be known for each calibration curve, but a metric of the contact resistance would be sufficient. These calibration curves would require data from the deployed DTS system and independently logging θ sensors to be developed. A range of θ and contact resistance conditions would also be required, so it may take a year or longer to capture sufficient data to create the full range of calibration curves for a given soil type and θ regime. It may be possible to artificially replicate these conditions at different sections of a transect, such as covering the ground with an impermeable material to prevent infiltration and create more extreme dry conditions. It is also important to note the normal error distribution used in the error propagation analysis is somewhat high in comparison to other DTS systems. Some DTS systems have reported accuracies of 0.01°C compared to the 0.1°C of the Halo DTS system, which would improve the values in Table 3.1. Initial error propagation results suggest an accuracy of 0.01°C would improve the RMSE of the two proposed data interpretation techniques from 0.075 and 0.082 to 0.019 and 0.027, respectively.

3.5. Conclusion

Two promising methods have been introduced to estimate θ with heated DTS technology despite the presence of a spatially and temporally dependent contact resistance. The first method is to develop an estimate of the contact resistance by analyzing the early time data of the heating and cooling phase. It may also be advantageous to analyze several small heat

pulses prior to a long heat pulse to obtain several estimates of the contact resistance. Once the contact resistance is parameterized, θ can be estimated by developing calibration curves of a maximum temperature response metric (e.g. ΔT_{55}) versus θ for different contact resistances.

The second method is to analyze late time data to estimate θ independent of the contact resistance by fitting a line to the temperature response against log time. This method is more convenient, but requires a sufficiently long heat pulse. The required duration will depend on the cable design and magnitude of contact resistance. Both methods are prone to error associated with random instrumental noise and possibly error associated with ambient temperature drift, water movement, and vapor movement. Future work is required to test these data interpretation techniques on actual data, but there are some initial findings using the error propagation analysis. This analysis showed that both methods were not accurate given noise with a standard deviation of 0.05°C, although the method that estimated θ after parameterizing contact resistance was more robust than the method that estimated θ from the late time slope. Both methods were somewhat accurate at $\theta < 0.30$ (RMSE=0.062 and RMSE=0.069). These uncertainties do not seem acceptable for a θ sensor, but would likely approach acceptable levels with a temperature resolution improvement. Beyond improving the temperature resolution, small heat pulses could be used to improve the parameterization of contact resistance, which would further improve that method of estimating θ.

Tables & Figures

Table 3.1. RMSE values using the two proposed methods to estimate θ from synthetic temperature response curves with random noise from a normal distribution and a standard deviation of 0.05°C.

Method	**All simulations**	**θ < 0.30**	**θ ≥ 0.30**
Using CR estimate	0.075	0.062	0.086
Late time slope	0.082	0.069	0.094

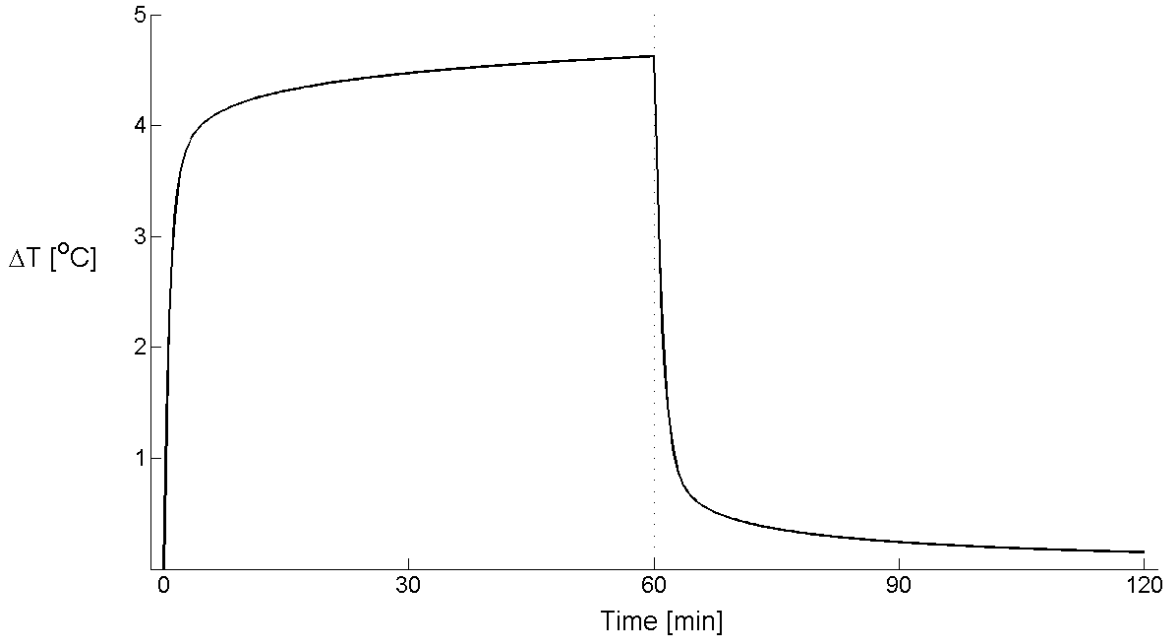

Fig. 3.1: Model results of a 60 minute heat pulse followed by a 60 minute cooling phase.

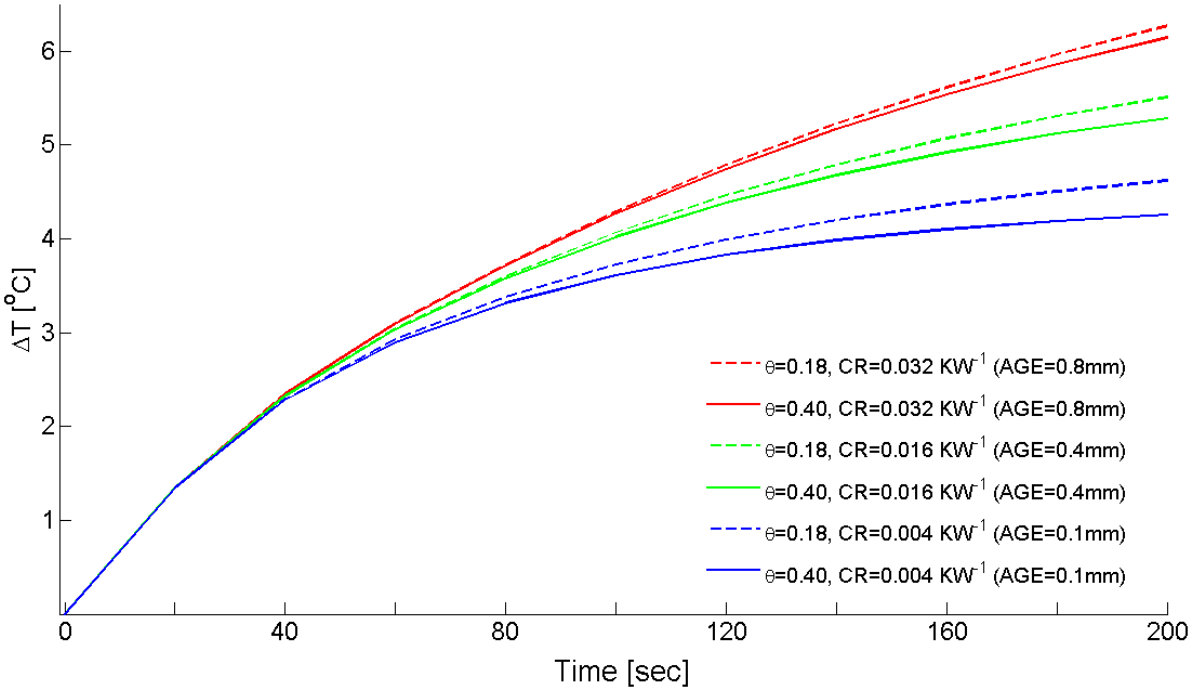

Fig. 3.2: Model results of 3 contact resistance conditions under the two extreme θ conditions (0.18 and 0.40).

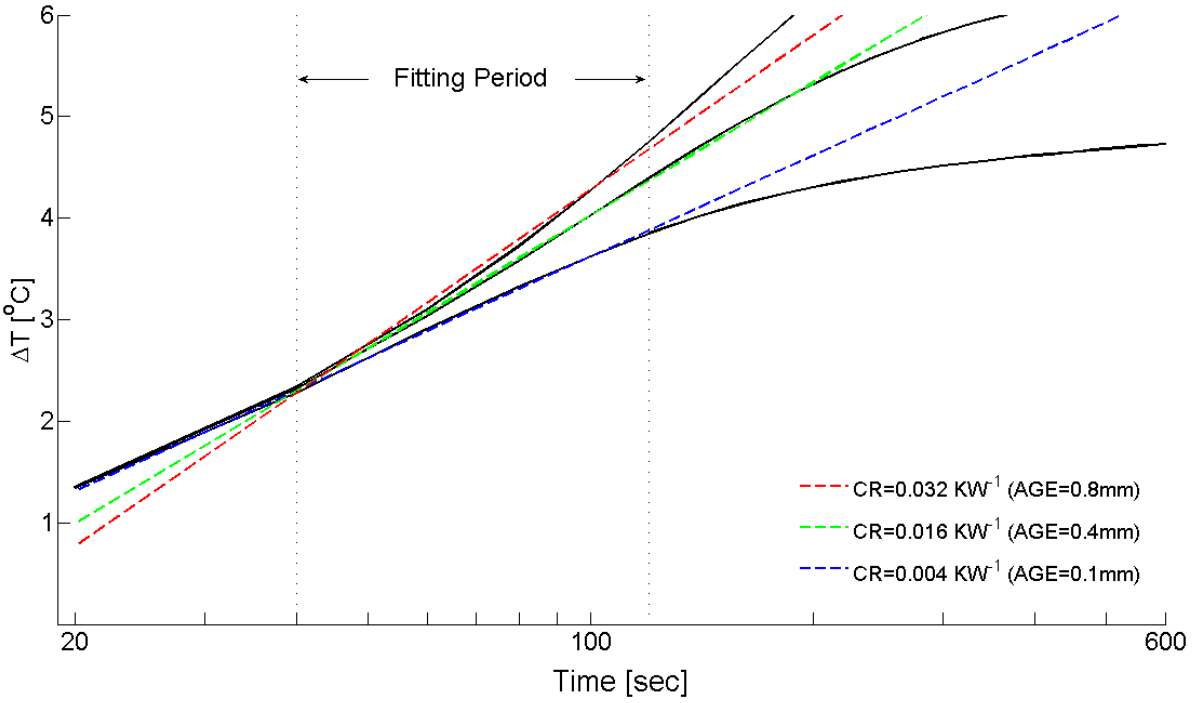

Fig. 3.3: Model results of three contact resistance conditions at one θ condition with the x-axis on a log scale. The temperature response is approximately linear through log time during the fitting period, which was defined as 40 to 120 seconds after the heat pulse began. Linear functions were fit to the data within this period. This process was completed for all 759 model simulations, but only 3 simulations are shown to simplify the visual.

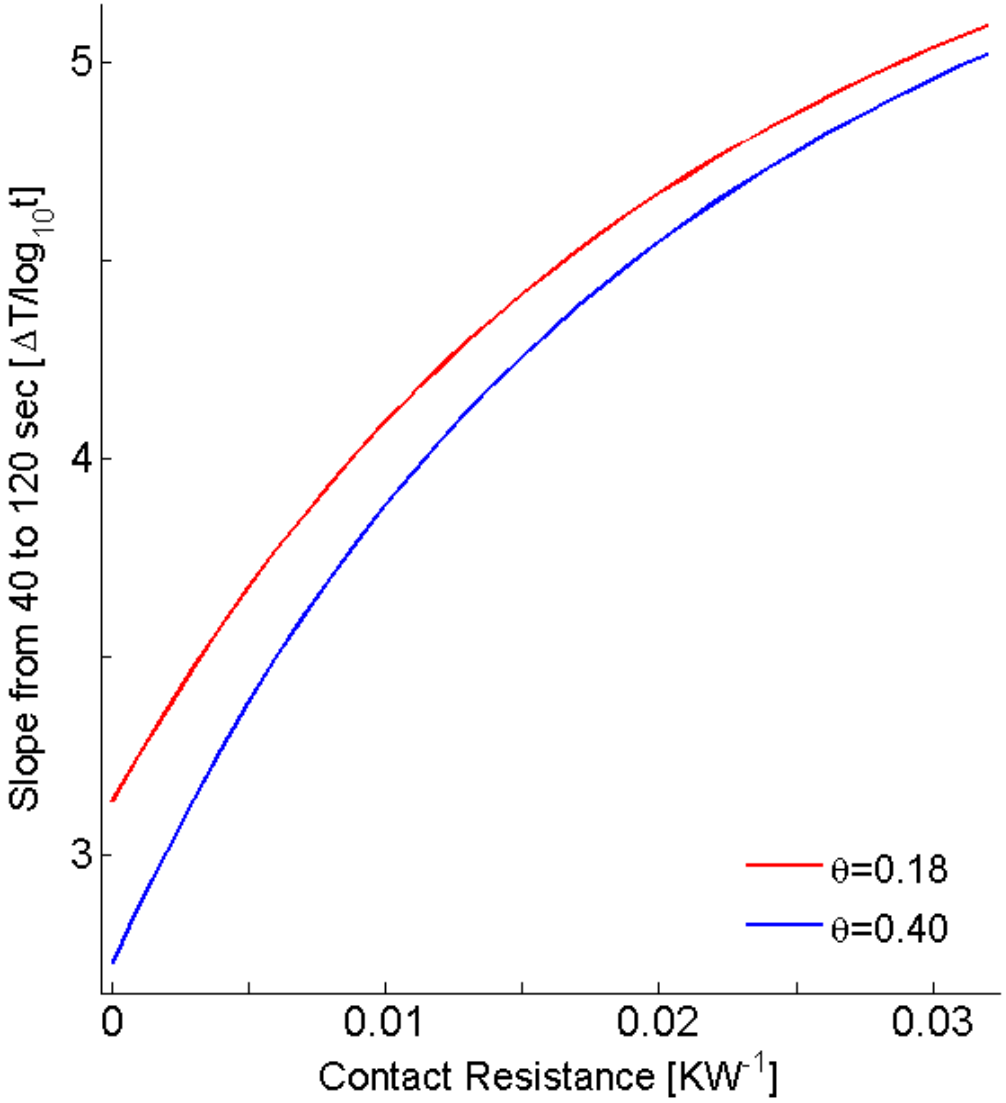

Fig. 3.4: The results of the fitted linear functions from Figure 3.3 are shown. The slope of these lines is plotted against the contact resistance. Only results from the two extreme θ conditions are shown to simplify the visual. The slope of all other θ conditions falls between these two lines.

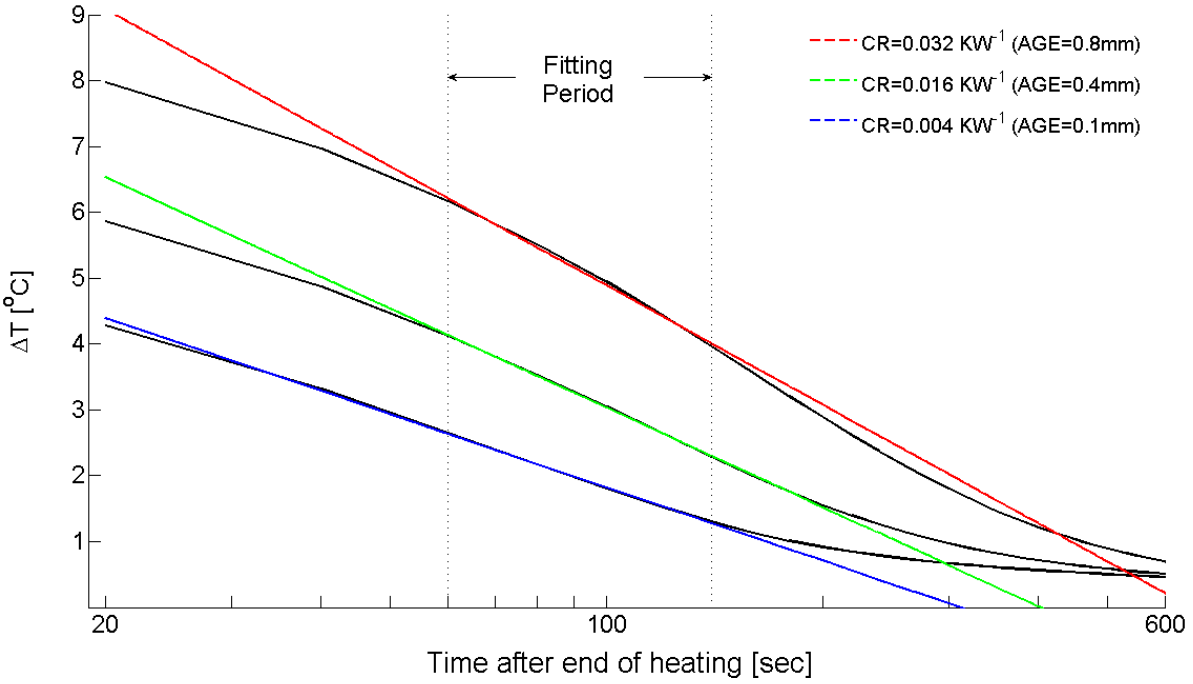

Fig. 3.5: Model results of the first 10 minutes of the cooling phase with time on a log scale. Three contact resistance conditions are shown for one θ condition to simplify the visual (this process was completed for all 759 model simulations). Linear functions were fit to the temperature response during the fitting period, which was defined as 60 to 140 seconds after the end of the heat pulse.

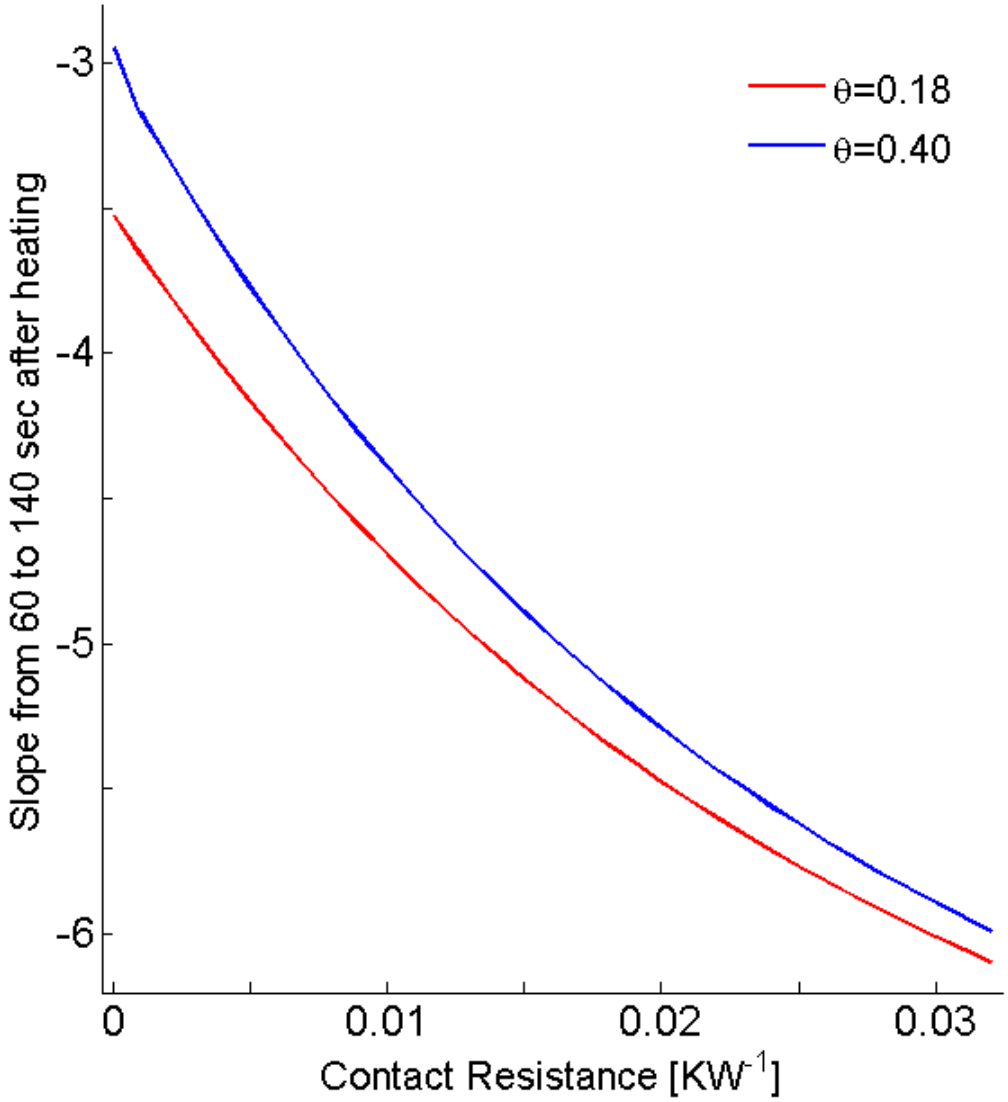

Fig. 3.6: The results of the fitted linear functions from Figure 3.5 are shown. The slope of these lines is plotted against the contact resistance. Only results from the two extreme θ conditions are shown to simplify the visual. The slope of all other θ conditions falls between these two lines.

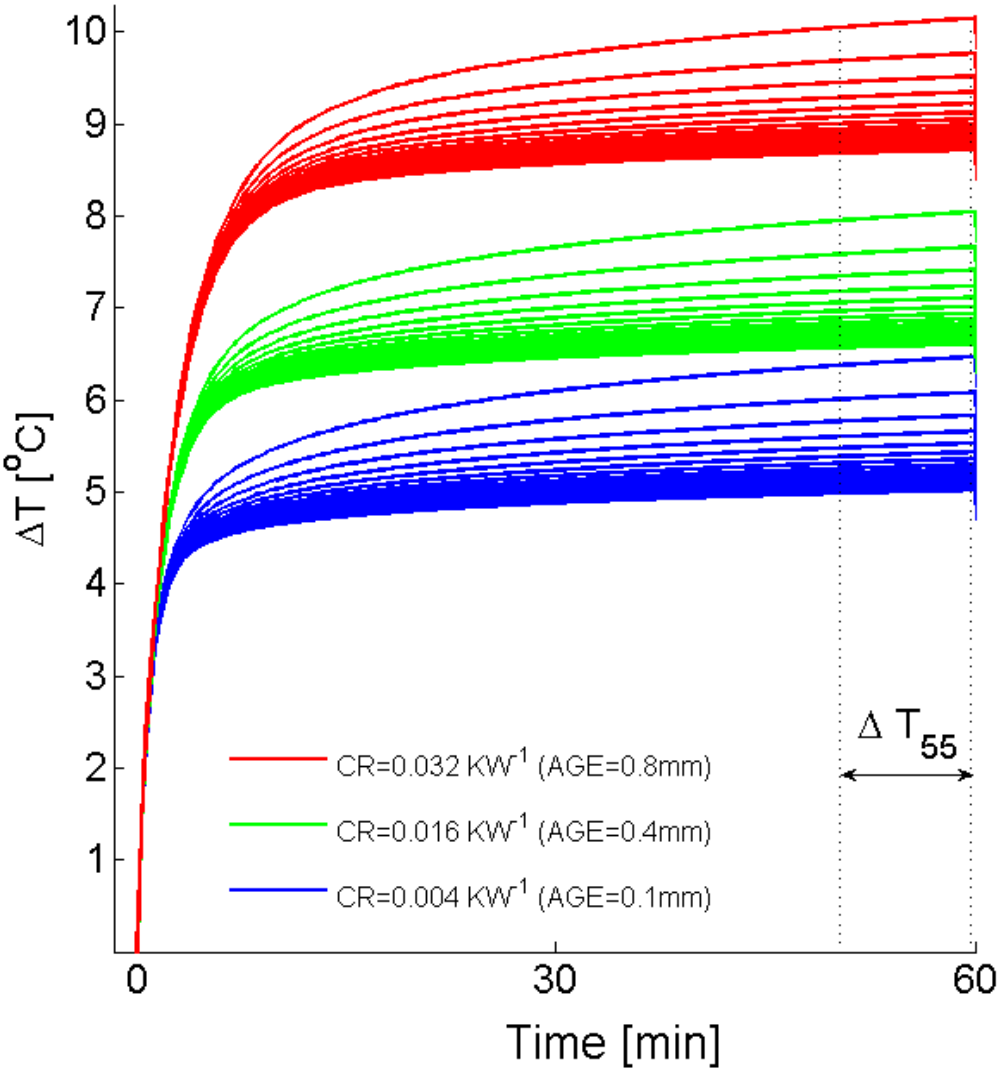

Fig. 3.7: Model results of the temperature response during the heating phase of three contact resistance conditions with all θ conditions. A maximum temperature response metric (ΔT_{55}) was defined as the average temperature response from 50 to 60 minutes.

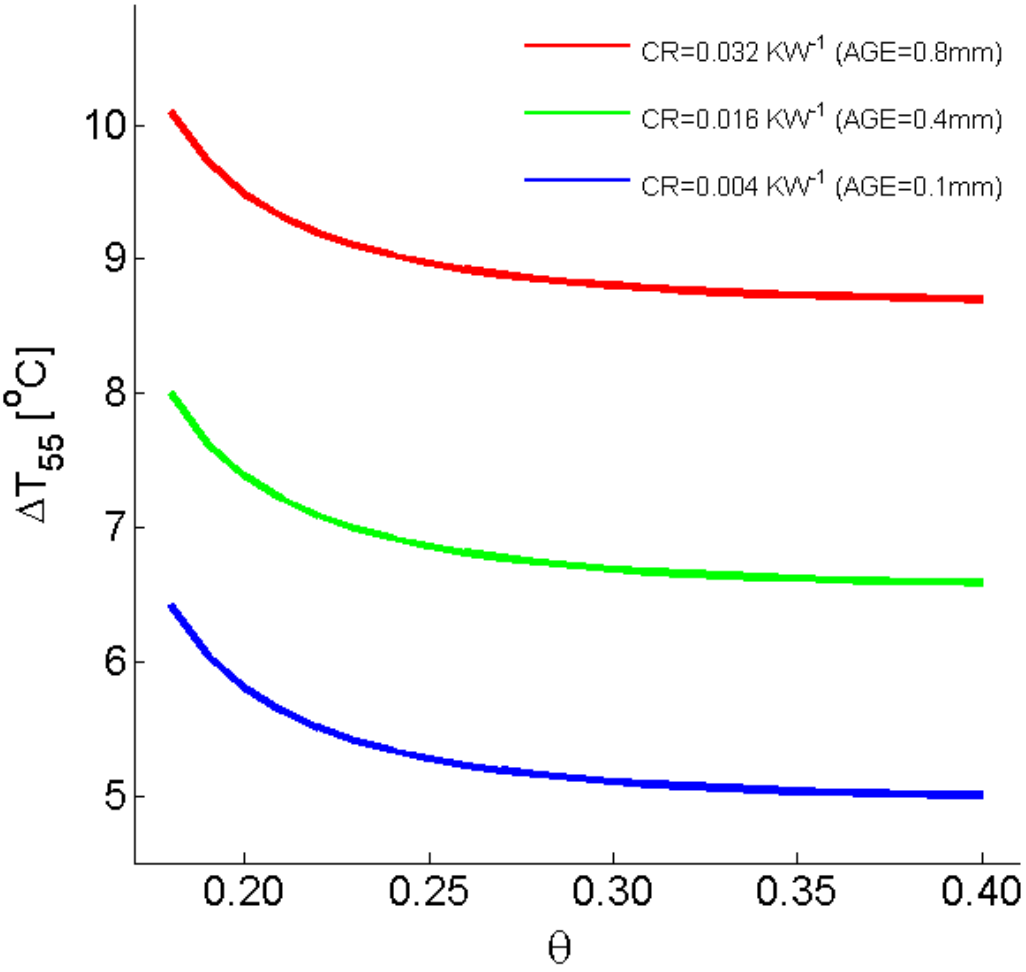

Fig. 3.8: ΔT_{55} from the results shown in Figure 3.7 are plotted against θ for the three contact resistance conditions.

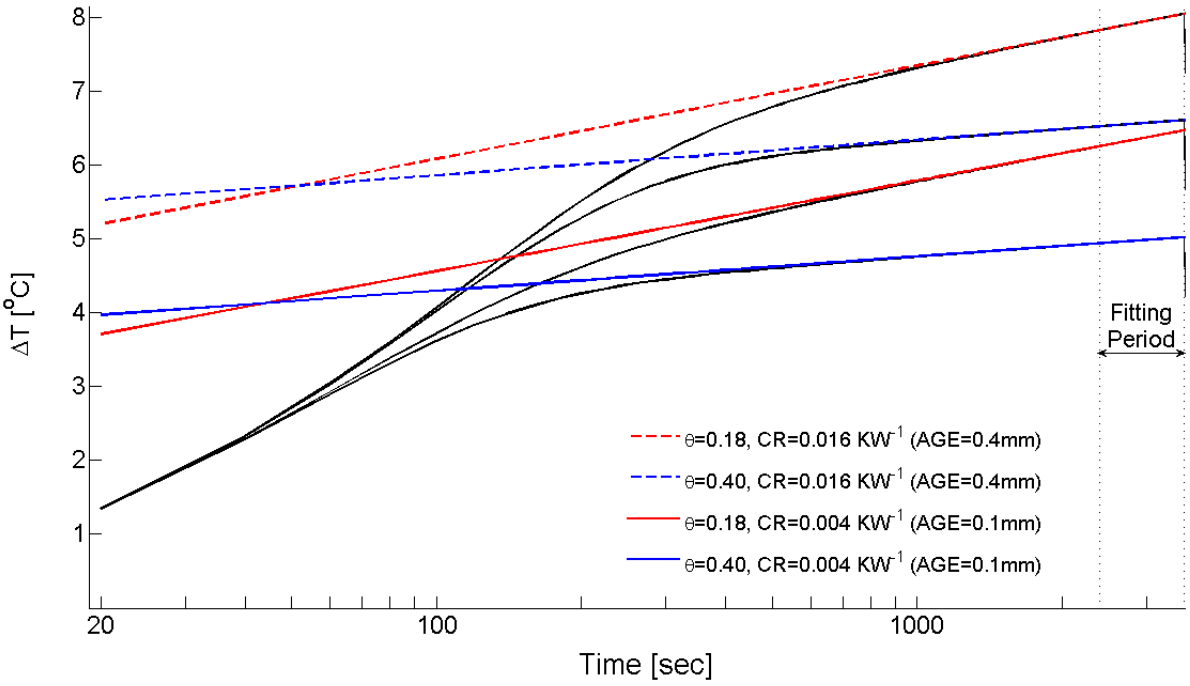

Fig. 3.9: Model results are shown for the temperature response of two contact resistance conditions at the two extreme θ conditions versus log time. Linear functions were fit to the temperature response during the fitting period, which was defined as 40 to 60 minutes into the heat pulse.

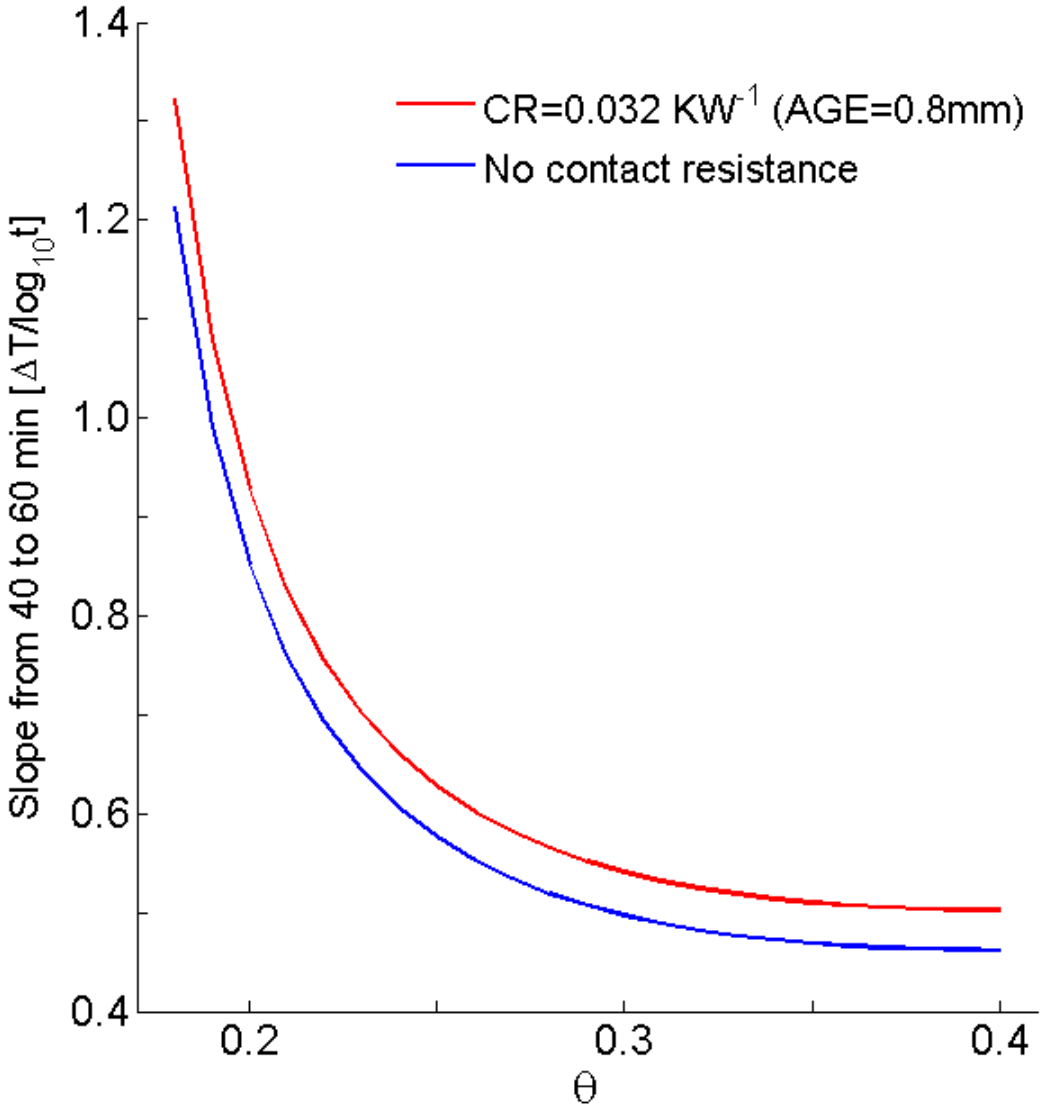

Fig. 3.10: The results of the fitted linear functions from Figure 3.9 are shown. The slope of these lines is plotted against θ. Only results from the two extreme contact resistance conditions are shown to simplify the visual. The slope of all other contact resistance conditions falls between these two lines.

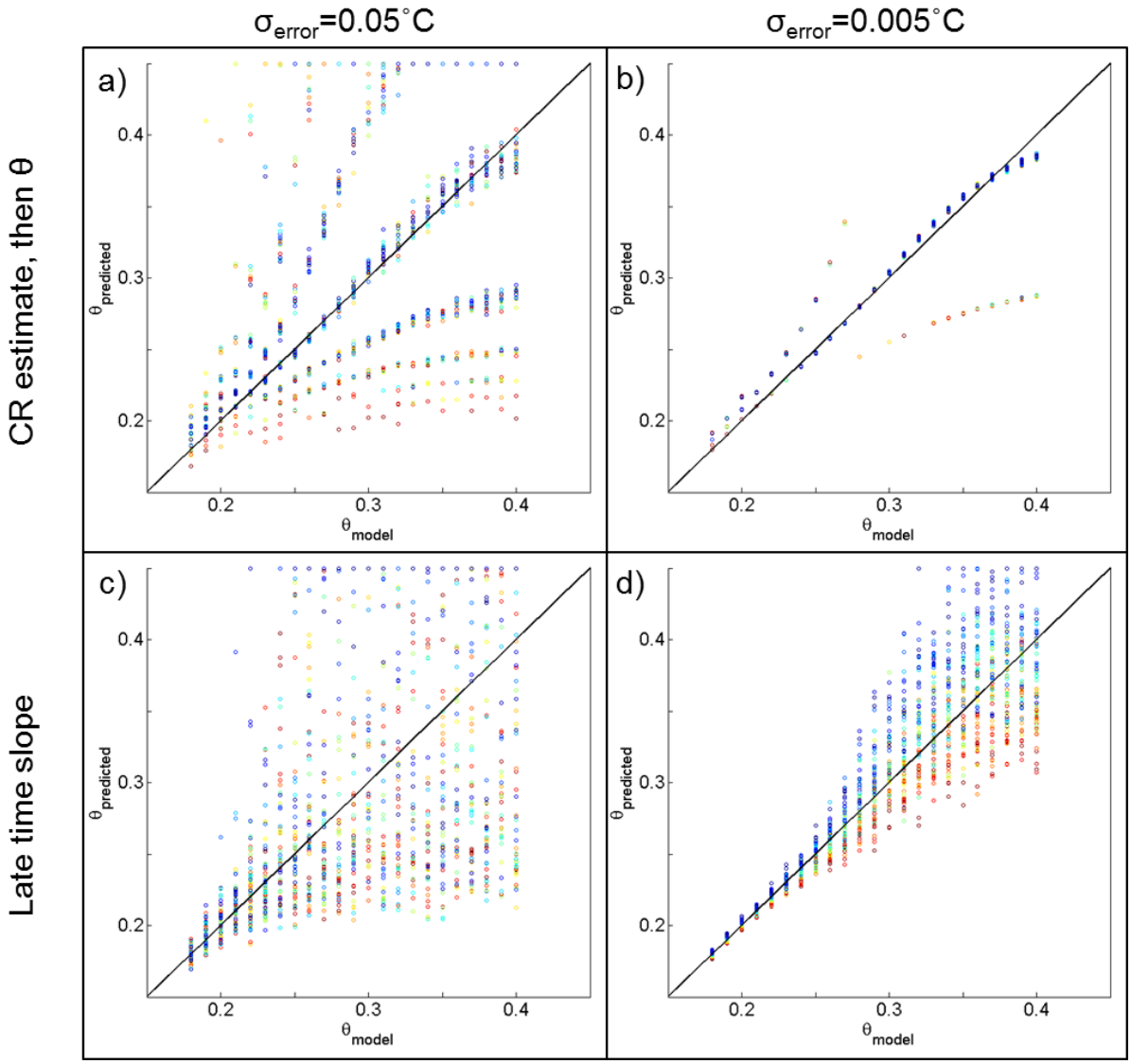

Fig. 3.11: Results of the error propagation analysis for both data interpretation techniques with a normal error distribution and a standard deviation of 0.05˚C and 0.005˚C. Contact resistance is color-coded with red representing a large contact resistance and blue representing a small contact resistance.

Chapter 4: Conclusion & Future Work

4.1. Conclusions

A heated DTS system deployed during the summer of 2010 at the East Branch Pecatonica River Hydroecologic Observatory has provided several insights into the feasibility of using this technology to estimate θ. The initial data interpretation process was to correlate a metric of temperature response (ΔT_8) within the cable with independently logging dielectric θ sensors to develop a calibration curve. This calibration curve did not behave as predicted by model results. There were three primary mechanisms identified causing this deviation.

One mechanism was a θ-dependent contact resistance. As the soil dried, the contact resistance between the cable and soil increased based on model simulations. This finding should actually create a more sensitive calibration curve, which is desirable, but the relationship between θ and contact resistance did not appear to be spatially uniform. If this relationship is spatially heterogeneous, then there would be a unique calibration for each section of the DTS cable. Developing separate calibration curves would require independent θ observations at every section of the cable, which would be expensive and time consuming. Another mechanism was hydrologically driven deviations from the expected calibration curve. The relationship between ΔT_8 and θ_{obs} was found to contain hysteretic behavior where the previous wetting and drying cycles influenced this relationship. This observation showed that multiple ΔT_8 responses could correspond to a given θ. Thermal hysteresis was not apparent with independently logging λ sensors, so it was concluded that this hysteresis was a result of the pore structure directly surrounding the cable. The third mechanism observed was

soil structure healing following the deployment of the cable into the ground. This mechanism caused the calibration curve to become less sensitive through time and approach the calibration curve predicted by the model results. It is important to note that these previous two mechanisms also appeared to vary in magnitude spatially (Appendix A).

These three mechanisms introduce significant complexity to the ΔT_8-θ relationship, but each one is related to the pore structure (i.e. air gaps or contact resistance) directly surrounding the cable. This commonality suggests these mechanisms should have a similar effect on the temperature response although possessing different dynamics. This realization inspired the pursuit of different techniques to interpret the temperature response. Two general techniques were proposed. The first technique involved parameterizing the contact resistance with early time heating and cooling phase data and then estimating θ using late time heating phase data. The other technique involved using the slope of late time data to estimate θ independent of the contact resistance, which is a common method to estimating λ and then correlating to θ (Shiozawa and Campbell, 1990). Both methods were found to be insensitive to θ changes in wet conditions ($\theta \geq 0.30$), but the first technique was found to provide more accurate θ estimates in the presence of random, instrumental noise. This technique also has a greater potential for improvement by better parameterizing the contact resistance.

4.2. Future Directions

Initial attempts at parameterizing the contact resistance with early time heating phase data and using this information to inform an estimate of θ has not produced accurate estimates of θ. This inaccuracy could be a result of insufficient early time data to accurately estimate the contact resistance, insufficient late time data to estimate θ, or complications caused other

variables (i.e. noise). The current 10-minute heat pulse could be increased to determine if more late time data improves estimates of θ. A longer heat pulse could also provide data to estimate θ independent of the contact resistance using the slope of late time data. Different heating durations should be tested as there is likely an optimum duration that provides a sufficient amount of data while minimizing errors associated with ambient temperature drift, water movement, and vapor movement. Methods to reduce random noise should be explored as an error propagation analysis found that the current temperature resolution is too large for either data interpretation method to accurately estimate θ. The temperature resolution could be improved by increasing the time interval between temperature readings, although this change has the obvious tradeoff of reducing the quantity of available data. Another option to improve the temperature resolution would be to use a better DTS processor. Initial error propagation results suggest a temperature resolution of 0.01°C would improve the RMSE of both proposed data interpretation techniques from 0.077 and 0.112 to 0.011 and 0.023, respectively.

Estimates of contact resistance could be improved by obtaining more data points during early parts of the heating and cooling phase by decreasing the time interval at which temperature readings are taken by the DTS system or decreasing the magnitude of the heat pulse, which will extend the period that is primarily dependent on the contact resistance. A smaller interval between temperature readings will introduce more noise, so this change would likely reduce the data quality at the expense of increasing the data quantity. Decreasing the magnitude of the heat pulse may not be an improvement either. A smaller heat pulse may

provide more data primarily dependent on the contact resistance, but it will also require longer durations to obtain data primarily dependent on θ. It may be advantageous to start with a low intensity heat pulse and then switch to a higher intensity heat pulse, but the current DTS system at the East Branch Pecatonica River Observatory is not capable of changing this variable during a heat pulse.

Better estimates of contact resistance could be obtained by inducing several short heat pulses, which sole purpose would be to estimate the contact resistance. With the current power input, these short heat pulses would only need to be approximately 2 minutes in duration. Each short heat pulse would provide estimates of the contact resistance from the heating and cooling phases. After several short heat pulses, a long heat pulse could be induced to provide data dependent on θ. Modeling should be completed to estimate the necessary time between short heat pulses to prevent previous heat pulses from affecting subsequent heat pulses. The combination of several short heat pulses and one long heat pulse should provide sufficient data to estimate the contact resistance and θ. The slope of the late time data could also be used to provide another estimate of θ, but this method may be more prone to uncertainly caused by noise and other environmental influences such as ambient temperature drift.

This work also helps to inform future DTS system designs. Most soil types are likely to have a θ-dependent contact resistance. Soil types with higher clay content will be more prone to shrinking under dry conditions, which magnifies the contact resistance. Many soils with complex pore structures will also have hysteretic behavior. Other DTS systems will also face the obstacle of installation while minimizing the soil disturbance. The DTS cable in this study was installed with a vibratory plow and wetted following installation to encourage

healing. Even with these precautions, the healing process appeared to last at least 2 years. The likely prevalence of these obstacles across soil types suggests data interpretation techniques that recognize contact resistances should be used.

Greater accuracy could be obtained with dual probe heated DTS systems. Dual probe heated DTS systems could provide estimates of heat capacity and λ to infer θ. Placing two cables in the ground at a constant distance along the entire length of the two cables would be the challenging aspect of implementing a dual probe DTS system. Contact resistances would still be an issue, but could be potentially overcome using similar data interpretation techniques proposed in Chapter 3.

Appendix A

Figures 2.8 and 2.9 displayed the results showing soil thermal hysteresis and soil structure healing, respectively. Both plots used θ_{obs} at Location D. The following figures display the same figures for the other five locations. The thermal hysteresis figures have a different number of tiles for each location. This difference was created by defining a wetting event as an increase in θ_{obs} of 0.002 over a 15 minute period. Some locations did not have the quick increase in θ_{obs} as others, so over the same time period, the number of wetting events varied by location. As for the soil structure healing figures, the primary drying periods were defined using Location D and used for the five locations. This method was used as the primary drying periods did not vary significantly between locations.

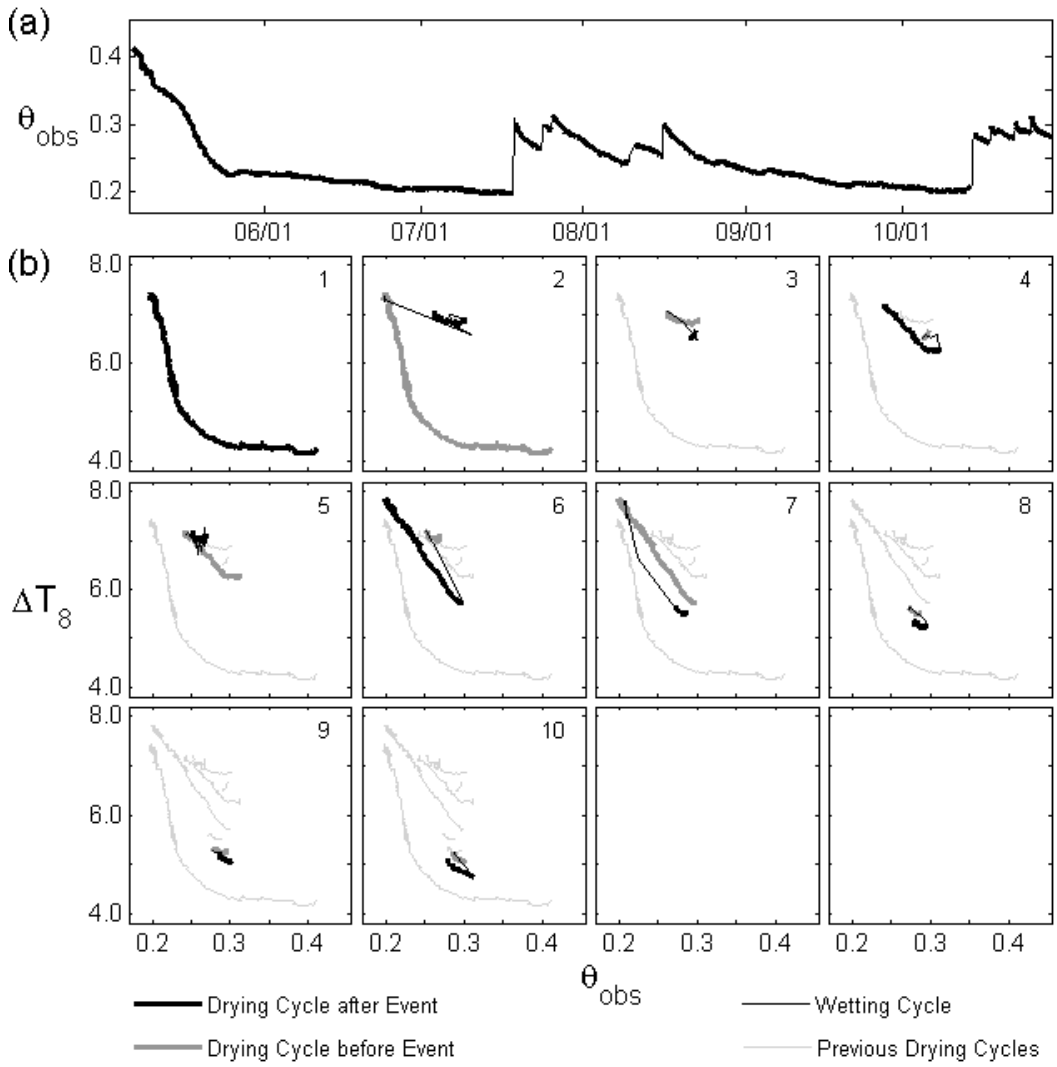

Figure A1: (a) shows the θ_{obs} time series from a dielectric sensor located at Location A along the DTS cable. (b) shows the corresponding ΔT_8 response (13 point moving average) at this location on the DTS cable versus the θ_{obs} graphed in (a). Each separate subplot within (b) represents a different wetting event (except for b-1, which displays the initial drying curve). Subplots display the drying curves prior to the wetting event in gray, wetting curves with a thin black line, drying curves following the wetting event in black, and all previous drying curves with thin gray lines.

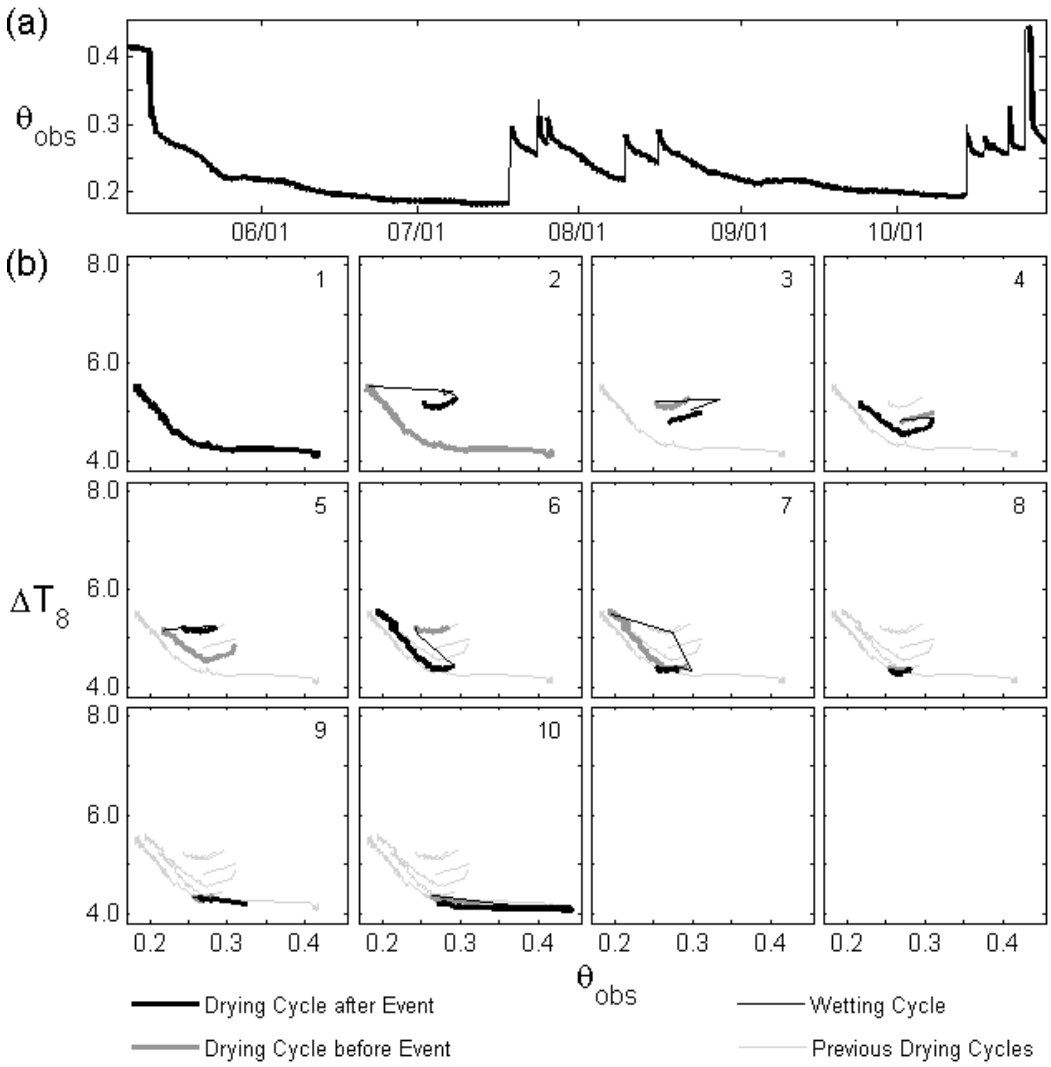

Figure A2: (a) shows the θ_{obs} time series from a dielectric sensor located at Location B along the DTS cable. (b) shows the corresponding ΔT_8 response (13 point moving average) at this location on the DTS cable versus the θ_{obs} graphed in (a). Each separate subplot within (b) represents a different wetting event (except for b-1, which displays the initial drying curve). Subplots display the drying curves prior to the wetting event in gray, wetting curves with a thin black line, drying curves following the wetting event in black, and all previous drying curves with thin gray lines.

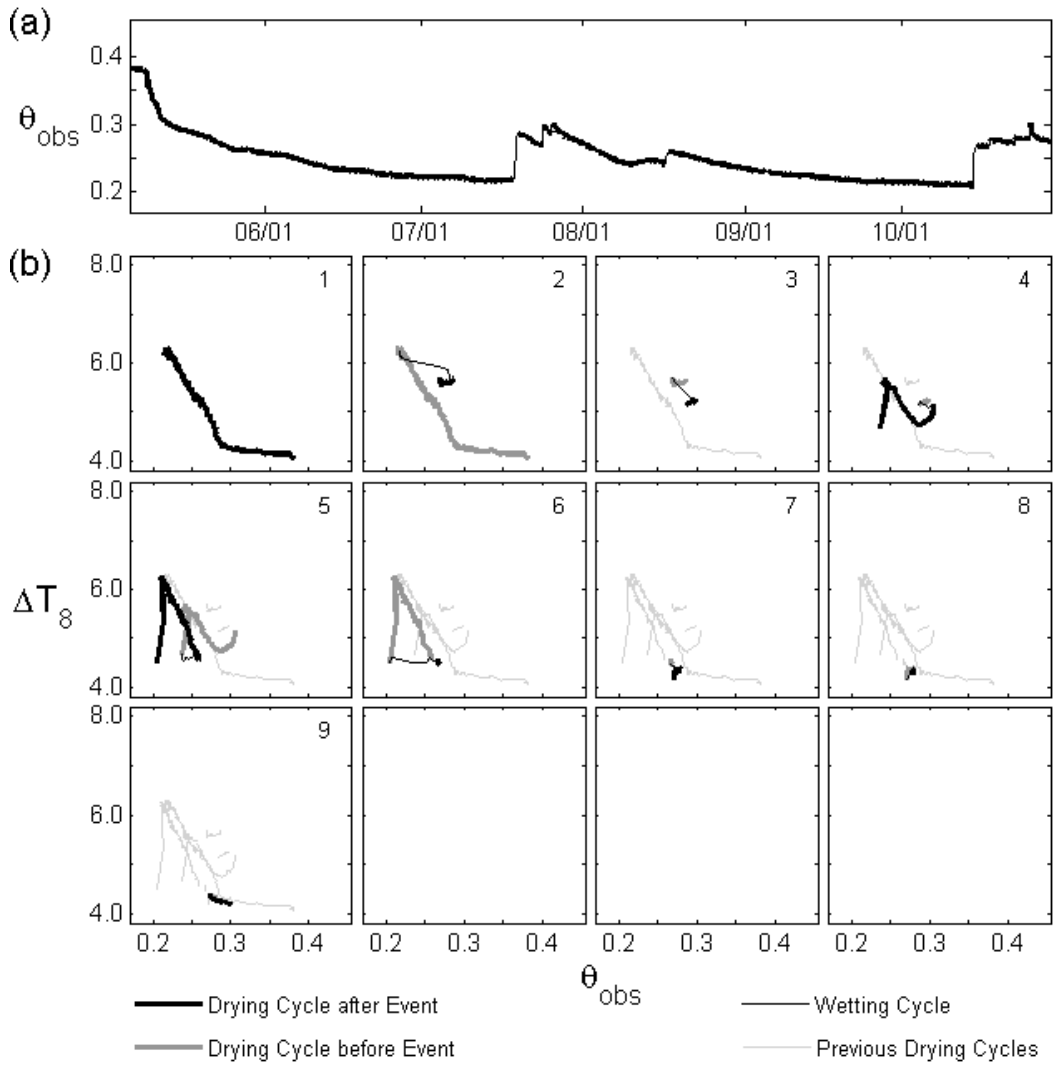

Figure A3: (a) shows the θ_{obs} time series from a dielectric sensor located at Location C along the DTS cable. (b) shows the corresponding ΔT_8 response (13 point moving average) at this location on the DTS cable versus the θ_{obs} graphed in (a). Each separate subplot within (b) represents a different wetting event (except for b-1, which displays the initial drying curve). Subplots display the drying curves prior to the wetting event in gray, wetting curves with a thin black line, drying curves following the wetting event in black, and all previous drying curves with thin gray lines.

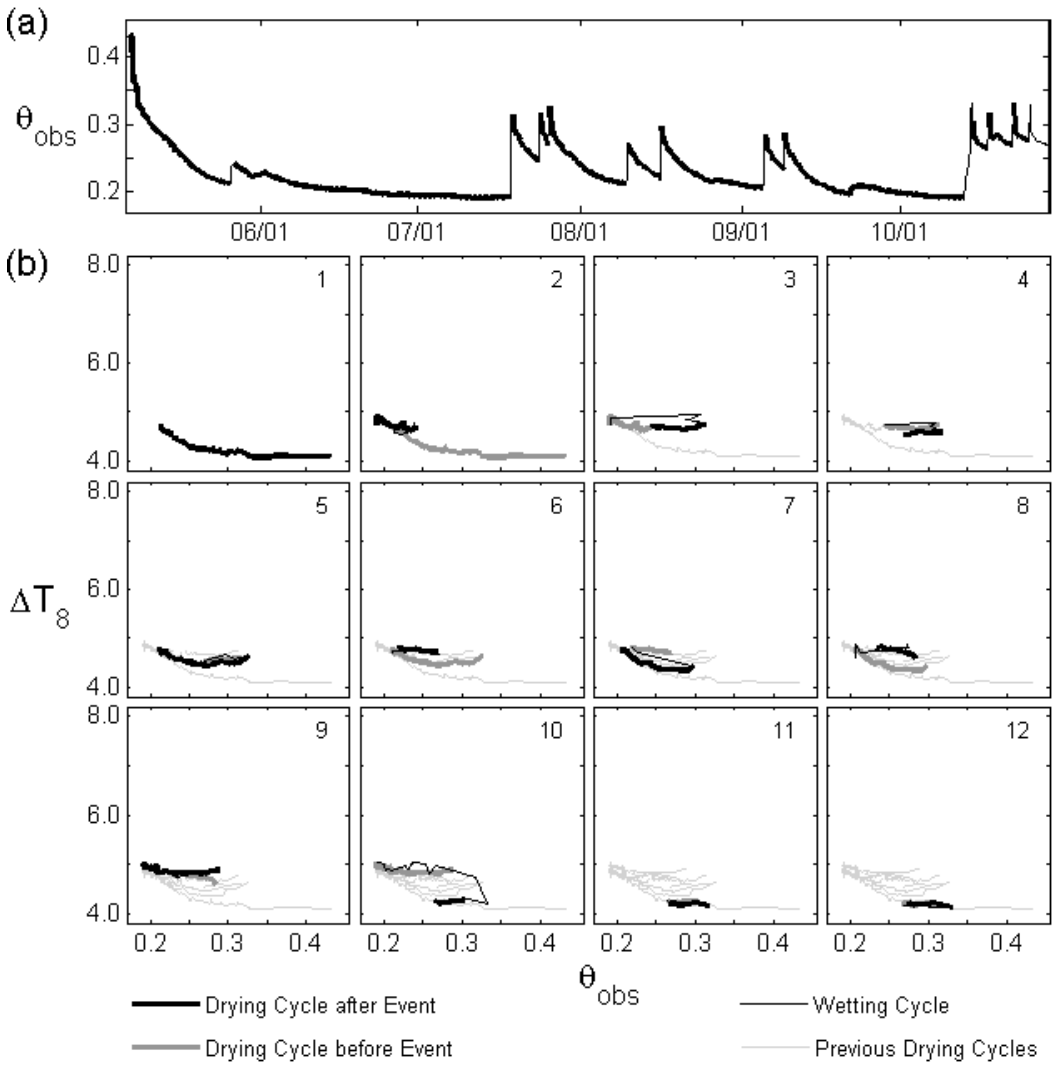

Figure A4: (a) shows the θ_{obs} time series from a dielectric sensor located at Location D along the DTS cable. (b) shows the corresponding ΔT_8 response (13 point moving average) at this location on the DTS cable versus the θ_{obs} graphed in (a). Each separate subplot within (b) represents a different wetting event (except for b-1, which displays the initial drying curve). Subplots display the drying curves prior to the wetting event in gray, wetting curves with a thin black line, drying curves following the wetting event in black, and all previous drying curves with thin gray lines.

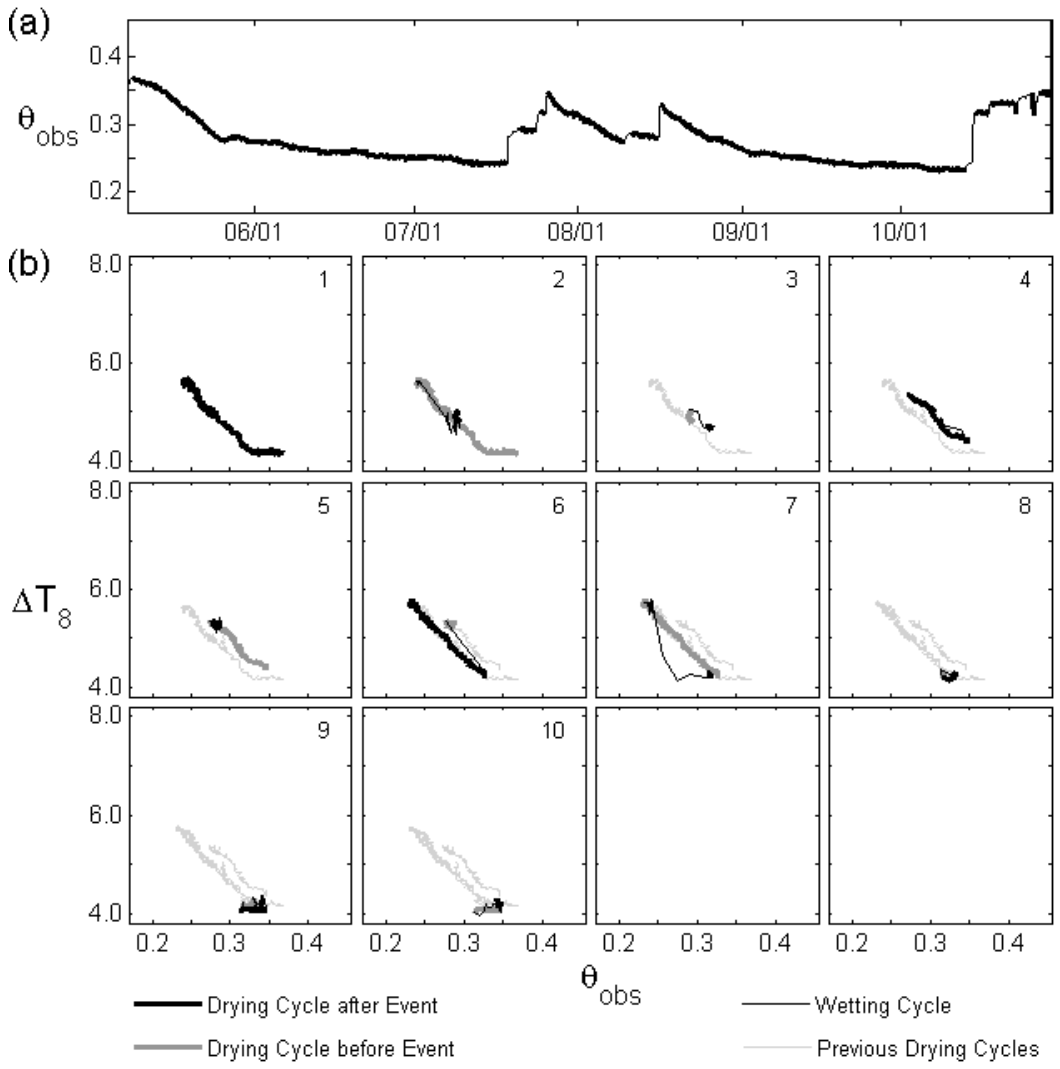

Figure A5: (a) shows the θ_{obs} time series from a dielectric sensor located at Location E along the DTS cable. (b) shows the corresponding ΔT_8 response (13 point moving average) at this location on the DTS cable versus the θ_{obs} graphed in (a). Each separate subplot within (b) represents a different wetting event (except for b-1, which displays the initial drying curve). Subplots display the drying curves prior to the wetting event in gray, wetting curves with a thin black line, drying curves following the wetting event in black, and all previous drying curves with thin gray lines.

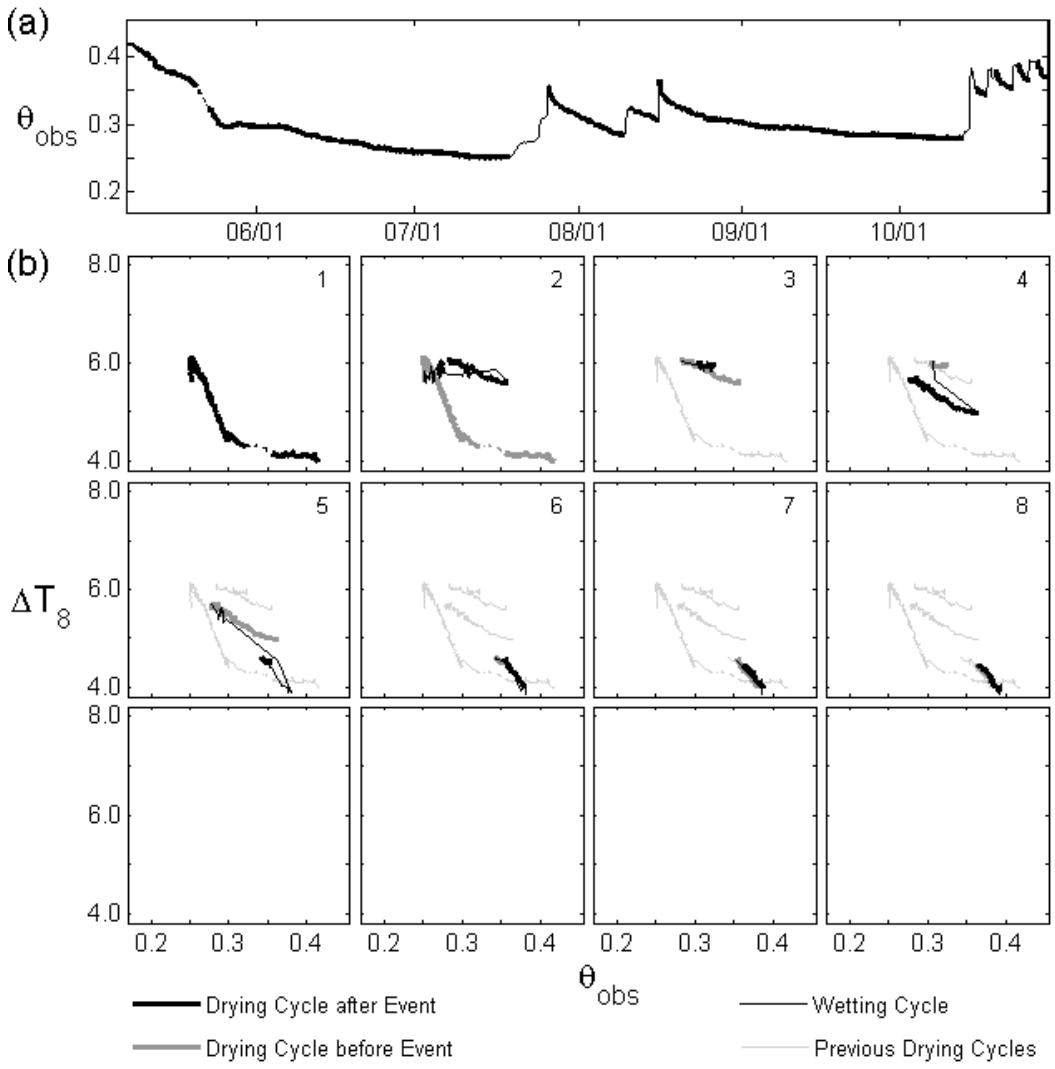

Figure A6: (a) shows the θ_{obs} time series from a dielectric sensor located at Location F along the DTS cable. (b) shows the corresponding ΔT_8 response (13 point moving average) at this location on the DTS cable versus the θ graphed in (a). Each separate subplot within (b) represents a different wetting event (except for b-1, which displays the initial drying curve). Subplots display the drying curves prior to the wetting event in gray, wetting curves with a thin black line, drying curves following the wetting event in black, and all previous drying curves with thin gray lines.

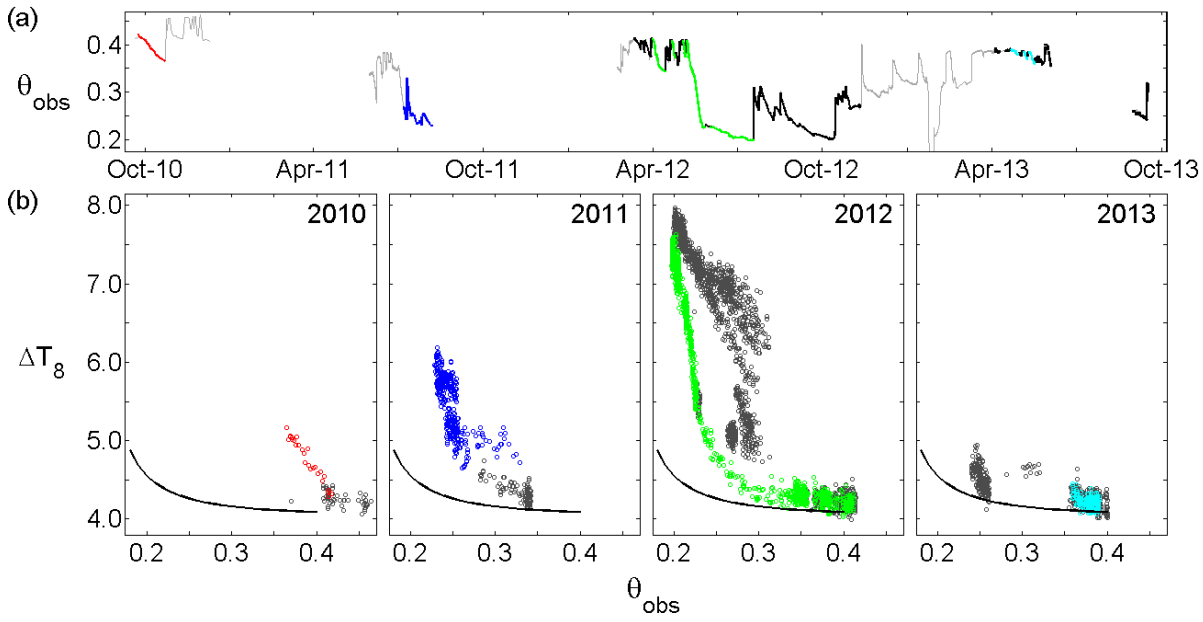

Figure A7: Data from a dielectric θ sensor located at Location A from September 2010 to September 2013 (a). Bold and colored sections represent data that have corresponding DTS data for that time period. Colored sections were highlighted because DTS data are available at those dates and these sections have dried from near saturation without any significant wetting events prior. These time periods should be minimally affected by soil thermal hysteresis. These sections have been grouped by year: 2010 (red), 2011 (blue), 2012 (green), and 2013 (turquoise). θ_{obs} data are paired with ΔT_8 data from the section of the DTS cable where this dielectric θ sensor is located (b). Time periods highlighted in (a) are also highlighted in (b). Remaining DTS data in bold sections in (a) are displayed in gray in (b).

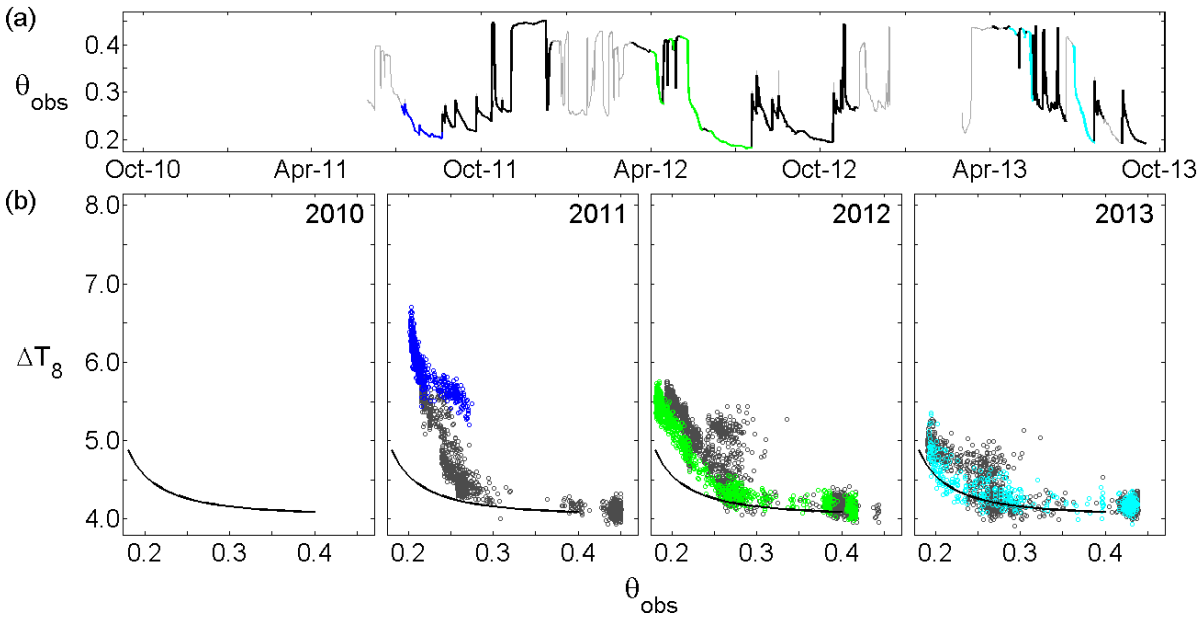

Figure A8: Data from a dielectric θ sensor located at Location B from May 2011 to September 2013 (a). Bold and colored sections represent data that have corresponding DTS data for that time period. Colored sections were highlighted because DTS data are available at those dates and these sections have dried from near saturation without any significant wetting events prior. These time periods should be minimally affected by soil thermal hysteresis. These sections have been grouped by year: 2011 (blue), 2012 (green), and 2013 (turquoise). θ_{obs} data are paired with ΔT_8 data from the section of the DTS cable where this dielectric θ sensor is located (b). Time periods highlighted in (a) are also highlighted in (b). Remaining DTS data in bold sections in (a) are displayed in gray in (b).

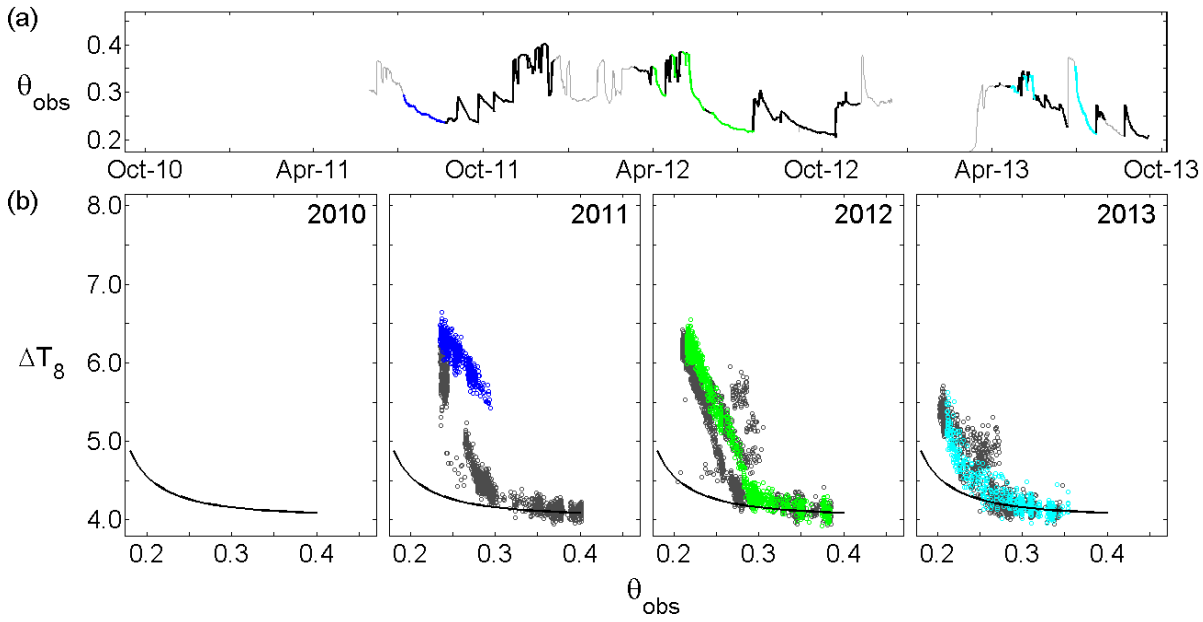

Figure A9: Data from a dielectric θ sensor located at Location C from May 2011 to September 2013 (a). Bold and colored sections represent data that have corresponding DTS data for that time period. Colored sections were highlighted because DTS data are available at those dates and these sections have dried from near saturation without any significant wetting events prior. These time periods should be minimally affected by soil thermal hysteresis. These sections have been grouped by year: 2011 (blue), 2012 (green), and 2013 (turquoise). θ_{obs} data are paired with ΔT_8 data from the section of the DTS cable where this dielectric θ sensor is located (b). Time periods highlighted in (a) are also highlighted in (b). Remaining DTS data in bold sections in (a) are displayed in gray in (b).

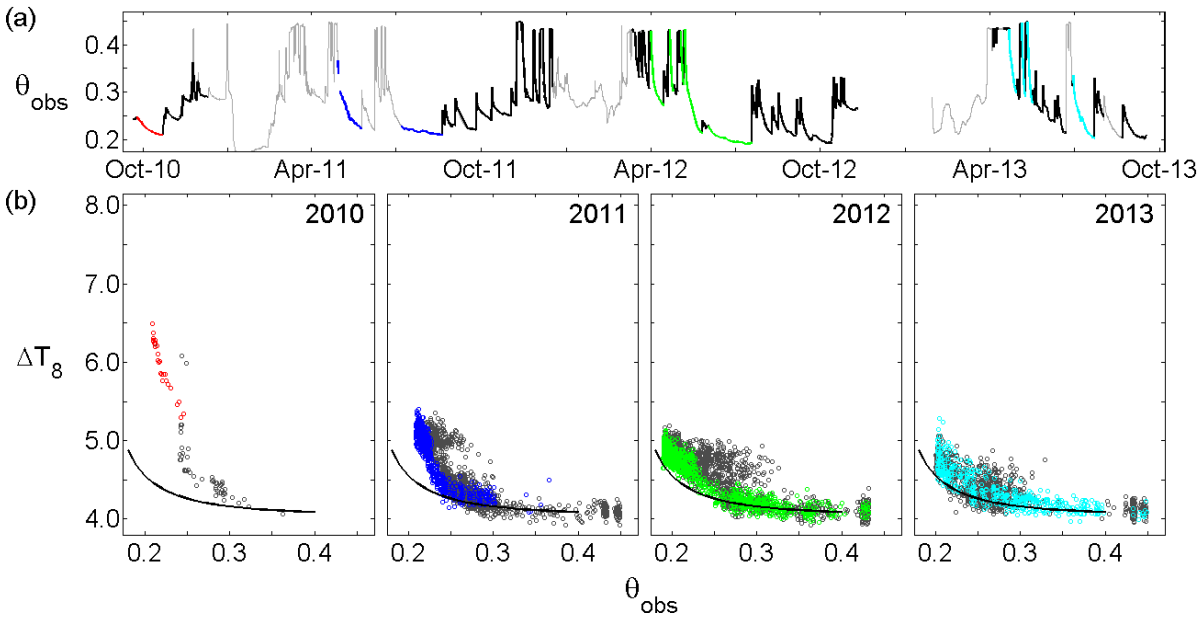

Figure A10: Data from a dielectric θ sensor located at Location D from September 2010 to September 2013 (a). Bold and colored sections represent data that have corresponding DTS data for that time period. Colored sections were highlighted because DTS data are available at those dates and these sections have dried from near saturation without any significant wetting events prior. These time periods should be minimally affected by soil thermal hysteresis. These sections have been grouped by year: 2010 (red), 2011 (blue), 2012 (green), and 2013 (turquoise). θ_{obs} data are paired with ΔT_8 data from the section of the DTS cable where this dielectric θ sensor is located (b). Time periods highlighted in (a) are also highlighted in (b). Remaining DTS data in bold sections in (a) are displayed in gray in (b).

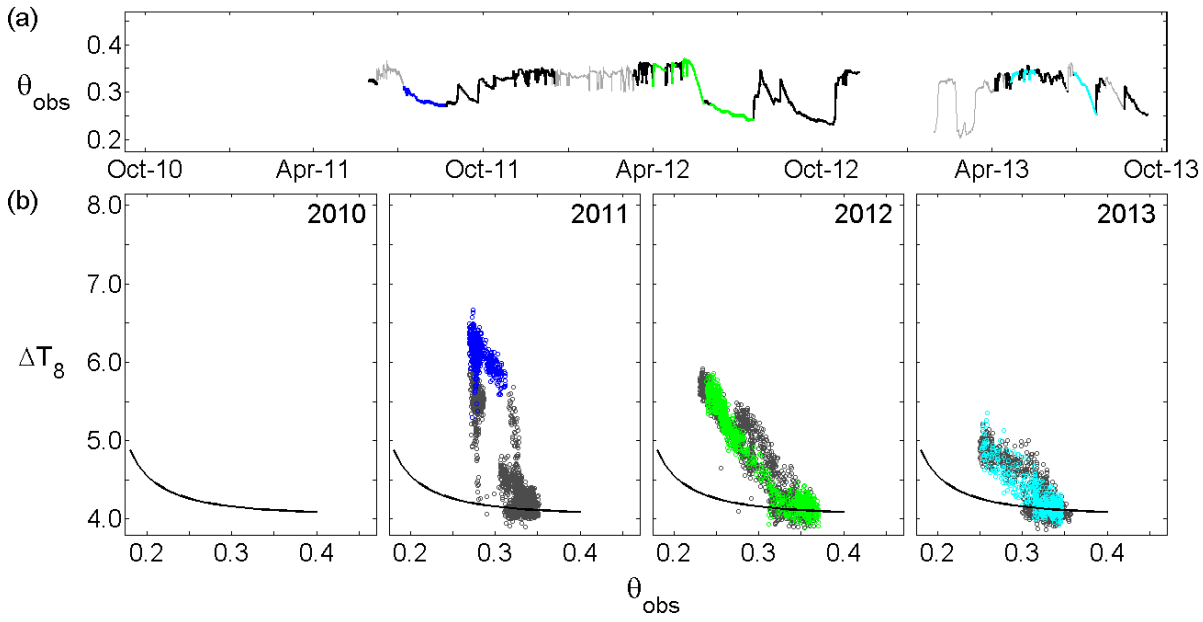

Figure A11: Data from a dielectric θ sensor located at Location E from May 2011 to September 2013 (a). Bold and colored sections represent data that have corresponding DTS data for that time period. Colored sections were highlighted because DTS data are available at those dates and these sections have dried from near saturation without any significant wetting events prior. These time periods should be minimally affected by soil thermal hysteresis. These sections have been grouped by year: 2011 (blue), 2012 (green), and 2013 (turquoise). θ_{obs} data are paired with ΔT_8 data from the section of the DTS cable where this dielectric θ sensor is located (b). Time periods highlighted in (a) are also highlighted in (b). Remaining DTS data in bold sections in (a) are displayed in gray in (b).

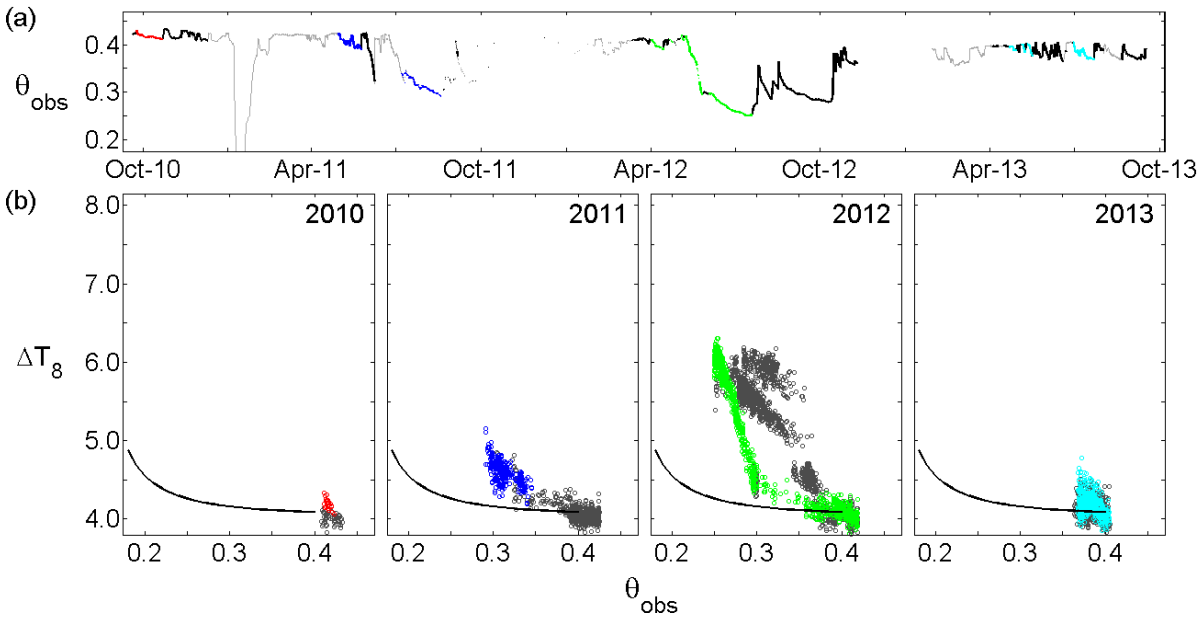

Figure A12: Data from a dielectric θ sensor located at Location F from September 2010 to September 2013 (a). Bold and colored sections represent data that have corresponding DTS data for that time period. Colored sections were highlighted because DTS data are available at those dates and these sections have dried from near saturation without any significant wetting events prior. These time periods should be minimally affected by soil thermal hysteresis. These sections have been grouped by year: 2010 (red), 2011 (blue), 2012 (green), and 2013 (turquoise). θ_{obs} data are paired with ΔT_8 data from the section of the DTS cable where this dielectric θ sensor is located (b). Time periods highlighted in (a) are also highlighted in (b). Remaining DTS data in bold sections in (a) are displayed in gray in (b).

References

Blackwell, J.H., 1954. A Transient-Flow Method for Determination of Thermal Constants of Insulating Materials in Bulk Part I—Theory. J. Appl. Phys. 25, 137.

Booth, E.G., Loheide, S.P., 2010. Effects of evapotranspiration partitioning, plant water stress response and topsoil removal on the soil moisture regime of a floodplain wetland: implications for restoration. Hydrol. Process. 24, 2934–2946.

Booth, E.G., Loheide, S.P., 2012a. Comparing surface effective saturation and depth-to-water-level as predictors of plant composition in a restored riparian wetland. Ecohydrology 5, 637–647.

Booth, E.G., Loheide, S.P., 2012b. Hydroecological model predictions indicate wetter and more diverse soil water regimes and vegetation types following floodplain restoration. J. Geophys. Res. 117, G02011.

Booth, E.G., Loheide, S.P., Hansis, R.D., 2009. Postsettlement Alluvium Removal: A Novel Floodplain Restoration Technique (Wisconsin). Ecol. Restor. 27, 136–139.

Bristow, K., White, R., Kluitenberg, G., 1994. Comparison of Single and Dual Probes for Measuring Soil Thermal Properties with Transient Heating. Aust. J. Soil Res. 32, 447–64.

Cardenas-Lailhacar, B., Dukes, M.D., Miller, G.L., 2008. Sensor-Based Automation of Irrigation on Bermudagrass , during Wet Weather Conditions 120–128.

Casper, M., Gemmar, P., Gronz, O., Johst, M., Stuber, M., 2007. Fuzzy logic-based rainfall — runoff modelling using soil moisture measurements to represent system state. Hydrol. Sci. J. 52, 478–490.

Chung, S.-O., Horton, R., 1987. Soil Heat and Water Flow With a Partial Surface Mulch. Water Resour. Res. 23, 2175–2186.

Ciocca, F., Lunati, I., Van de Giesen, N., Parlange, M.B., 2012. Heated Optical Fiber for Distributed Soil-Moisture Measurements: A Lysimeter Experiment. Vadose Zo. J. 11.

Dakin, J.P., Pratt, D.J., Bibby, G.W., Ross, J.N., 1985. Distributed optical fiber Raman temperature sensor using a semiconductor light-source and detector. Electron. Lett. 21, 569–570.

De Vries, D.A., 1952. A Nonstationary Method For Determining Thermal Conductivity of Soil in situ. Soil Sci. 73, 83–89.

De Vries, D.A., 1963. Thermal properties of soils. North-Holland Publishing Company, Amsterdam.

De Vries, D.A., Peck, A.J., 1958. On the cylindrical probe method of measuring thermal conductivity with special reference to soils. Part 1: Extension of theory and discussion of probe characteristics. Aust. J. Phys. 11, 255–271.

Dunne, T., Black, R.D., 1970. An Experimental Investigation Runol Production. Water Resour. Res. 6, 478–490.

Farouki, O.T., 1981. Thermal properties of soils, CRREL Mono. ed, Highway Research Board Special Report. Cold Regions Research and Engineering Laboratory, Hanover, NH.

García, A., Contreras, E., Domínguez, B., 1991. Developments in geothermal energy in Mexico: 33. Simultaneous determination of the thermal properties of geothermal drill cores. Heat Recover. Syst. CHP 11, 131–139.

Goto, S., Matsubayashi, O., 2008. Inversion of needle-probe data for sediment thermal properties of the eastern flank of the Juan de Fuca Ridge. J. Geophys. Res. 113, B08105.

Ham, J.M., Benson, E.J., 2003. On the Construction and Calibration of Dual-Probe Heat Capacity Sensors 1185–1190.

Heitman, J.L., Basinger, J.M., Kluitenberg, G.J., Ham, J.M., Frank, J.M., Barnes, P.L., 2003. Field Evaluation of the Dual-Probe Heat-Pulse Method for Measuring Soil Water Content. Vadose Zo. J. 2, 552–560.

Hunt, R.J., Jackson, J.O., Running, G.L., Krabbenhoft, D.P., J.T., K., 1999. Hydrogeological, geomorphological, and vegetative investigations of selected wetland creation and restoration projects, Report No. ed. U.S. Geological Survey, Wisconsin Department of Transportation, Federal Highway Administration, Washington D.C.

Kerr, Y.H., Waldteufel, P., Wigneron, J.-P., Martinuzzi, J., Font, J., Berger, M., 2001. Soil moisture retrieval from space: the Soil Moisture and Ocean Salinity (SMOS) mission. IEEE Trans. Geosci. Remote Sens. 39, 1729–1735.

Khire, M. V, Benson, C.H., Bosscher, P.J., 1997. Water Balance Modeling of Earthern Final Covers. J. Geotech. Geoenvironmental Eng. 123, 744–754.

Knapp, A.K., Fay, P. a, Blair, J.M., Collins, S.L., Smith, M.D., Carlisle, J.D., Harper, C.W., Danner, B.T., Lett, M.S., McCarron, J.K., 2002. Rainfall variability, carbon cycling, and plant species diversity in a mesic grassland. Science 298, 2202–5.

Knox, J.C., 1972. Valley alluvation in southwestern Wisconsin. Ann. Assoc. Am. Geogr. 62, 401–410.

Knox, J.C., 2006. Floodplain sedimentation in the Upper Mississippi Valley: Natural versus human accelerated. Geomorphology 79, 286–310.

Krzeminska, D.M., Steele-Dunne, S.C., Bogaard, T. a., Rutten, M.M., Sailhac, P., Geraud, Y., 2012. High-resolution temperature observations to monitor soil thermal properties as a proxy for soil moisture condition in clay-shale landslide. Hydrol. Process. 26, 2143–2156.

Loheide, S.P., Booth, E.G., 2011. Effects of changing channel morphology on vegetation, groundwater, and soil moisture regimes in groundwater-dependent ecosystems. Geomorphology 126, 364–376.

Mortensen, A.P., Hopmans, J.W., Mori, Y., Šimůnek, J., 2006. Multi-functional heat pulse probe measurements of coupled vadose zone flow and transport. Adv. Water Resour. 29, 250–267.

Ochsner, T., Horton, R., Ren, T., 2001. A new perspective on soil thermal properties. Soil Sci. Soc. Am. … 65, 1641–1647.

Ochsner, T.E., Cosh, M.H., Cuenca, R.H., Dorigo, W. a., Draper, C.S., Hagimoto, Y., Kerr, Y.H., Njoku, E.G., Small, E.E., Zreda, M., 2013. State of the Art in Large-Scale Soil Moisture Monitoring. Soil Sci. Soc. Am. J.

Perzlmaier, S., Auñeger, M., Conrad, M., 2004. Distributed fiber optic temperature mesurements in hydraulic engineering - Prospects of the heat-up method, in: 72nd ICOLD Annual Meeting Workshop on Dam Safety Problems and Solutions-Sharing Experience, Korean Natl. Comm. on Large Dams. Seoul, Korea.

Perzlmaier, S., Straer, K.H., Strobl, T., Auñeger, M., 2006. Integral seepage monitoring on open channel embankment dams dy the DFOT heat pulse method, in: 74th Annual Meeting, Int. Comm. on Large Dams. Barcelona, Spain.

Robinson, D. a., Campbell, C.S., Hopmans, J.W., Hornbuckle, B.K., Jones, S.B., Knight, R., Ogden, F., Selker, J., Wendroth, O., 2008. Soil Moisture Measurement for Ecological and Hydrological Watershed-Scale Observatories: A Review. Vadose Zo. J. 7, 358.

Sayde, C., Gregory, C., Rodriguez, M.G., Tufillaro, N., Giesen, N. Van De, English, M., Cuenca, R., John, S., Gil-Rodriguez, M., Tyler, S., van de Giesen, N., Selker, J.S., 2010. Feasibility of soil moisture monitoring with heated fiber optics. Water Resour. Res. 46, n/a–n/a.

Selker, J.S., Thévenaz, L., Huwald, H., Mallet, A., Luxemburg, W., Van De Giesen, N., Stejskal, M., Zeman, J., Westhoff, M., Parlange, M.B., 2006. Distributed fiber-optic temperature sensing for hydrologic systems. Water Resour. Res. 42, 1–8.

Shaw, B., Baver, L.D., 1940. An Electrothermal Method for Following Moisture Changes of the Soil in Situ. Soil Sci. Soc. Am. J. 4, 78–83.

Shiozawa, S., Campbell, G.S., 1990. Soil Thermal Conductivity. Remote Sens. Rev. 5, 301–310.

Song, Y., Ham, J., Kirkham, M., Kluitenberg, G., 1998. Measuring Soil Water Content Under Turfgrass Using the Dual Probe Heat Pulse Technique. J. Am. Soc. Hortic. Sci. 123, 937–941.

Stafford, J. V, 2000. Implementing Precision Agriculture in the 21st Century. J. Agric. Eng. Res. 76, 267–275.

Steele-Dunne, S.C., Rutten, M.M., Krzeminska, D.M., Hausner, M., Tyler, S.W., Selker, J., Bogaard, T. a., Van De Giesen, N.C., 2010. Feasibility of soil moisture estimation using passive distributed temperature sensing. Water Resour. Res. 46, 1–12.

Striegl, A.M., 2011. Development and field implementation of a distributed soil moisture sensor using heated fiber optics. University of Wisconsin - Madison.

Striegl, A.M., Loheide, S.P., 2012. Heated distributed temperature sensing for field scale soil moisture monitoring. Ground Water 50, 340–7.

Suárez, F., Hausner, M.B., Dozier, J., Selker, J.S., Tyler, S.W., 2011. Heat Transfer in the Environment : Development and Use of Fiber-Optic Distributed Temperature Sensing, in: Developments in Heat Transfer. InTech.

Van Haneghem, I. a., 1983. An Improved Nonsteady State Probe Method For Measurements In Granular Materials - Experimental Results. High Temp. - high Press. 15, 367–74.

Waite, W.F., Gilbert, L.Y., Winters, W.J., Mason, D.H., 2006. Estimating thermal diffusivity and specific heat from needle probe thermal conductivity data. Rev. Sci. Instrum. 77, 044904.

Waite, W.F., Stern, L. a., Kirby, S.H., Winters, W.J., Mason, D.H., 2007. Simultaneous determination of thermal conductivity, thermal diffusivity and specific heat in sI methane hydrate. Geophys. J. Int. 169, 767–774.

Weiss, J.D., 2003. Using Fiber Optics to Detect Moisture Intrusion into a Landfill Cap Consisting of a Vegetative Soil Barrier. J. Air Waste Manag. Assoc. 1995 53, 1130–1148.

Youngs, E.G., 1956. A laboratory method of following moisture content changes. Trans. 6th Int. Congr. Soil Sci. B, 89–93.

Zhang, N., Wang, M., Wang, N., 2002. Precision agriculture * a worldwide overview 36, 113–132.